Probabilistic Engineering Mechanics 64 (2021) 103128

Contents lists available at ScienceDirect

Probabilistic Engineering Mechanics

journal homepage: www.elsevier.com/locate/probengmech

3rd-order Spectral Representation Method: Simulation of multi-dimensional random fields and ergodic multi-variate random processes with fast Fourier transform implementation

Lohit Vandanapu, Michael D. Shields *

Department of Civil & Systems Engineering, Johns Hopkins University, United States of America

ARTICLE INFO

Keywords:
Stochastic fields
Random fields
Spectral representation
Fast Fourier transform
Simulation

ABSTRACT

This paper introduces a generalized 3rd-order Spectral Representation Method for the simulation of multi-dimensional random fields and ergodic multi-variate stochastic processes with asymmetric non-linearities. The formula for the simulation of general d-dimensional random fields is presented and the method is applied to simulate 2D and 3D random fields. The differences between samples generated by the proposed methodology and the existing classical Spectral Representation Method are analysed. The formula for the simulation of multi-variate random processes is subsequently developed. An important feature of the methodologies is that they can be implemented efficiently with the Fast Fourier Transform (FFT), details of which are presented. Computational savings are shown to grow exponentially with dimensionality as a testament of the scalability of the simulation methodology. Examples highlighting the salient features of these methodologies are also presented.

1. Introduction

Stochastic processes and random fields are used extensively in engineering, from studying the dynamics of wind [1,2], ocean waves [3,4], and seismic loads [5] on structures to simulation of material microstructures [6,7]. Because of their importance, numerous methods have been developed for the simulation of stochastic processes and random fields. Simulation is particularly useful in the context of Monte Carlo simulations of large, complex non-linear systems where analytical analysis of the uncertainty in the system is not possible. Moreover, simulation of stochastic processes and random fields finds applications beyond simple Monte Carlo simulations and is important for essentially any simulation-based uncertainty quantification framework.

Until recently, simulation methods for stochastic processes and random fields have been derived only from second-order properties of the process or field. Consider a standard probability space $(\Omega, \mathcal{F}, \mathcal{P})$ where Ω is the sample space, $\mathcal{F}$ the sigma algebra of events, and $\mathcal{P}$ a probability measure. In these simulation methods, the process/field indexed on $\boldsymbol{x} \in D$ is represented in terms of a stochastic expansion of the general form

$$A(\boldsymbol{x}, \omega) \approx \hat{A}(\boldsymbol{x}, \omega) = \sum_{i=1}^{n} \theta_i(\omega)\psi_i(\boldsymbol{x}) \tag{1}$$

where $\theta_i(\omega), \omega \in \Omega$ are independent random variables and $\psi_i(\boldsymbol{x}), \boldsymbol{x} \in D$ are deterministic basis functions. Many such stochastic expansions have been developed. Among these methods the most popular ones are the Spectral Representation method (SRM) [8–10] and the Karhunen–Loeve Expansion (KLE) [11,12]. Each of these methods operates by finding a set of random variables $\theta_i(\omega)$ along with a set of compatible basis functions $\psi(\boldsymbol{x})$ satisfying $C(\boldsymbol{x_1}, \boldsymbol{x_2}) = \mathbb{E}[A(\boldsymbol{x_1})A(\boldsymbol{x_2})] = \mathbb{E}[\hat{A}(\boldsymbol{x_1})\hat{A}(\boldsymbol{x_2})]$.

For the SRM, $\psi_i(\boldsymbol{x})$ are the harmonic functions (Fourier basis) and $\theta_i(\omega)$ are random variables whose amplitude is derived from the power spectrum (Fourier transform of the covariance function $C(\boldsymbol{x_1}, \boldsymbol{x_1})$). Likewise for the K-L expansion, $\psi_i(\boldsymbol{x})$ are the eigen-functions of the covariance function and $\theta_i(\omega)$ are standard normal random variables scaled by the square root of the appropriate eigenvalues.

While each of these methods has its advantages, all such methods have a common disadvantage in that they are only second-order representative, i.e they can only match the process up to its covariance function. Unless acted upon by a nonlinear operator, these fields are asymptotically Gaussian as the number of terms n increases [13]. In signal processing terms, the stochastic processes and random fields simulated by the above methods are equivalent to the output of a linear system acted upon by Gaussian random noise. This simplification breaks down in case of real world scenarios such as seismic waves propagating through different strata of soil, non-linear wind loads on structures, ocean waves acting on an off-shore structural system, or turbulent flow of a fluid governed by the Navier–Stokes equation. Thus, the second-order representation inherently limits these methods

* Corresponding author.
E-mail address: michael.shields@jhu.edu (M.D. Shields).

https://doi.org/10.1016/j.probengmech.2021.103128
Received 7 October 2020; Received in revised form 14 January 2021; Accepted 1 March 2021
Available online 14 March 2021

as they fail to match the higher order properties of the stochastic fields, which dominate the tail behaviour and in turn plays a crucial role in uncertainty quantification, reliability etc. The stochastic fields generated from these non-linear systems possess asymmetric non-linear wave interactions which need to be included in the stochastic expansion, details of which were first introduced in [14] and are reviewed in the subsequent sections.

Methods for the simulation of non-Gaussian stochastic fields work primarily through a non-linear transformation of the stochastic expansion in Eq. (1). One class of such nonlinear transformations works by introducing correlated random variables with deterministic basis functions such as Hermite and Legendre polynomials [15,16]. These stochastic processes match the marginal statistical moments to a certain order along with the covariance function. Perhaps the most commonly used method is the explicit Cumulative Distribution Function (CDF) based transformation [17,18] given by

$$Y(x) = F^{-1}(\Phi(A(x))) \tag{2}$$

where $A(x)$ is a standard Gaussian random process, $\Phi(\cdot)$ is the standard normal CDF and $F^{-1}(\cdot)$ is the inverse CDF of the prescribed non-Gaussian distribution. This method is generally referred to as the 'translation process'. Efficient algorithms for the translation of scalar, vector, stationary, and non-stationary stochastic processes simulated by either SRM or KLE method have been developed in recent years [2,19–21]. Another class of methods for simulation of non-Gaussian stochastic processes are based on polynomial-chaos expansions [22]. Also, wavelet-based simulation methodologies have been developed and applied extensively in the case of non-stationary stochastic processes [23,24].

In this work, we are interested in the simulation of multidimensional random fields and multi-variate stochastic processes (stochastic vector processes). As a brief note, stochastic processes and random fields here are considered probabilistically equivalent with the only difference being that stochastic processes are indexed on time (one-dimensional, denoted by t or τ, with ω representing frequency under a Fourier transform) while random fields are indexed on space (denoted by x or ξ, with κ representing wave-number under a Fourier transform). Thus, multi-dimensional random fields are specifically indexed on multiple spatial dimensions, while stochastic vector processes are composed of multiple correlated random processes, generally occurring at different discrete spatial locations.

Generally speaking, the simulation of stochastic vector processes poses the larger technical challenges given its spatial and temporal dependence. Methods for simulation of multi-dimensional random fields, on the other hand, often follow as a natural extensions of their one-dimensional counterparts, although this is not the case for the higher-order processes we study here. Several methods, dating back nearly 50 years, have been proposed for the simulation of multi-dimensional random fields and stochastic vector processes including methods for stationary, non-stationary, Gaussian and non-Gaussian processes. Much of this began with the seminal work of Shinozuka who proposed the Spectral Representation method (SRM) in the early 1970s [25]. Later, in the late 1980s, Mignolet and Spanos [26,27], in a 2-part paper, introduced the recursive simulation of stationary multivariate stochastic processes based on autoregressive moving averages methods. This was followed by numerous works in the 1990s, when much of the theory for the SRM was developed. Li and Kareem [28] developed a framework for the simulation of non-stationary multivariate processes with the use of a stochastic decomposition technique and later developed a hybrid discrete Fourier Transform and digital filtering approach [29]. With regard to the SRM, Shinozuka and Deodatis developed the theoretical framework for simulation of ergodic, Gaussian stochastic vector processes [30] and multi-dimensional Gaussian random fields [31] in 1996, with subsequent extensions to non-stationary [5] and non-Gaussian processes [32]. More recently, the Iterative Translation Approximation Method (ITAM) has been proposed for the efficient simulation of non-Gaussian stochastic vector translation processes by Shields and Deodatis [33]. Very recently, Liu et al. [34], proposed a novel method based on the combination of SRM with a proper orthogonal decomposition for dimension reduction.

As previously mentioned, the existing simulation methods for multi-dimensional random fields and stochastic vector process, even those with non-Gaussian marginals, are inherently second-order in that they capture only the second-order correlation structure of the process/field. Here, we develop the framework for efficient simulation of non-Gaussian multi-dimensional random fields and multi-variate random processes. We specifically consider third-order, asymmetrically non-linear random processes (i.e. processes that possess quadratic phase interactions leading to an asymmetrically skewed distribution) prescribed by a known power spectrum and bispectrum. This extends the generalized third-order spectral representation method proposed in [14] to multiple spatial dimensions as well as multiple variables and introduces a fast Fourier transform (FFT) implementation of the simulation algorithm that greatly improves the computational efficiency.

2. Properties of random fields and random vector processes

Prior to introducing any concepts in simulation, it is important first to understand several important properties of random fields and random vector processes. In the interest of brevity we present only the spectral properties of random fields in this section. Other properties such as stationarity of random fields, cumulants and moments of random fields along with symmetry of correlation and spectral properties of random vector processes are discussed in the Appendix.

As discussed in [35,36], it is common and advantageous to work with random fields in the Fourier space. For our purposes, the Fourier domain provides a convenient setting for a nonlinear expansion of random fields that can be derived directly from the third-order spectra. Next, we review the spectral quantities necessary for the third-order expansion proposed herein.

The nth-order polyspectrum of a random field $A(x)$ is defined as the Fourier transform of its nth-order cumulant [35]

$$C_n^A(\kappa_1, \kappa_2, \dots, \kappa_{n-1}) = \frac{1}{(2\pi)^{n-1}} \int_{-\infty}^{\infty} \cdots \int_{-\infty}^{\infty} c_n^A(\xi_1, \xi_2, \dots, \xi_{n-1}) e^{\imath\kappa_1\xi_1 + \kappa_2\xi_2 + \cdots + \kappa_{n-1}\xi_{n-1}} d\xi_1 d\xi_2 \dots d\xi_{n-1} \tag{3}$$

The 2nd-order polyspectrum, also called the power spectrum and the 3rd-order polyspectrum, also called the bispectrum are of importance in this article. These are defined as follows:

$$S^A(\kappa) = C_2^A(\kappa) = \frac{1}{2\pi} \int_{-\infty}^{\infty} c_2^A(\xi) e^{-\imath(\kappa\xi)} d\xi \tag{4}$$

$$B^A(\kappa_1, \kappa_2) = C_3^A(\kappa_1, \kappa_2) = \frac{1}{(2\pi)^2} \int_{-\infty}^{\infty} \int_{-\infty}^{\infty} c_3^A(\xi_1, \xi_2) e^{-\imath(\kappa_1\xi_1 + \kappa_2\xi_2)} d\xi_1 d\xi_2 \tag{5}$$

The power spectrum expresses the power associated with each frequency component in the random field while the bispectrum describes nonlinear interaction between frequency pairs. The power spectrum is a real quantity while a bispectrum can have both real and imaginary parts. The real part of the bispectrum corresponds to the Fourier transform of the symmetric part of the third-order cumulant, whereas the imaginary part corresponds to the Fourier transform of the anti-symmetric part. As discussed by Lii et al. [37] and Elgar and Guza [3], the real component relates to the skewness of the field, while the imaginary component relates to the skewness of the derivative of the field. Meanwhile, the amplitude of the bispectrum represents the degree of quadratic phase coupling between the wave-numbers κ_1 and κ_2. A more detailed discussion can be found in [14] and [38].

For practical purposes, it is useful to normalize the polyspectrum, which introduces the notion of a polycoherence. Although several normalizations have been proposed [39–41], the nth-order squared

polycoherence is a standard measure of higher-order polyspectra, and is defined here for stationary random fields as

$$|\rho_A^{(n)}(\boldsymbol{\kappa})|^2 = \frac{\left|\mathbb{E}\left[\prod_{k=1}^{n-1} dZ(\kappa_k) dZ^*(\sum_{m=1}^{n-1}\kappa_m)\right]\right|^2}{\mathbb{E}\left[\prod_{k=1}^{n-1}|dZ(\kappa_k)|^2\right]\mathbb{E}\left[\left|dZ(\sum_{m=1}^{n-1}\kappa_m)\right|^2\right]} \tag{6}$$

where $dZ(\kappa)$ are the Fourier coefficients of the generalized random field and $*$ denotes the complex conjugate. Of particular interest here is the third-order polycoherence, or bicoherence which can be derived from Eq. (6) and is given by [39]:

$$b_A^2(\kappa_1,\kappa_2) = \frac{|B^A(\kappa_1,\kappa_2)|^2}{E[|dZ(\kappa_1)dZ(\kappa_2)|^2]S^A(\kappa_1+\kappa_2)} \tag{7}$$

where $dZ(\kappa)$ are the Fourier coefficients of $A(x)$, $B^A(\kappa_1,\kappa_2)$ is the bispectrum, and $S^A(\kappa)$ is the power spectrum. By Schwartz' inequality, this definition of the bicoherence is bounded on $[0,1]$ which provides a convenient interpretation of the fraction of energy associated with phase coupling. Further interpretation of the bicoherence can be found in [14,40,41]. Interestingly, the polycoherence also plays a crucial role in discriminating between non-linearity and non-stationarity in random fields [42].

3. Spectral representation theorem

Cramer's spectral representation [43] states that any zero-mean, weakly stationary random field $A(x)$ can be expressed in terms of a spectral process $z(\kappa)$ through the following Fourier–Stieltjes integral

$$A(x) = \int_{-\infty}^{\infty} e^{\imath\kappa x} dz(\kappa) \tag{8}$$

where the spectral process $z(\kappa)$ satisfies certain orthogonality conditions [44]. More generally, for a zero-mean, kth-order stationary ($k \geq 2$) random field $A(x)$, a spectral process $z(\kappa)$ can be assigned which satisfies Eq. (8), but possesses the following additional kth-order orthogonality properties [45]

$$\begin{aligned}
&\mathbb{E}[dz(\kappa)] = 0\\
&\mathbb{E}[z(\kappa)] = 0\\
&\mathbb{E}[|z(\kappa)|^2] = F(\kappa)\\
&\mathbb{E}[|dz(\kappa)|^2] = dF(\kappa)\\
&\mathbb{E}[z(\kappa_1)z(\kappa_2)z^*(\kappa_3)] = \delta(\kappa_1+\kappa_2-\kappa_3)G(\kappa_1,\kappa_2)\\
&\mathbb{E}[dz(\kappa_1)dz(\kappa_2)dz^*(\kappa_3)] = \delta(\kappa_1+\kappa_2-\kappa_3)dG(\kappa_1,\kappa_2)\\
&\vdots\\
&\mathbb{E}[z(\kappa_1)z(\kappa_2)\dots z^*(\kappa_k)] = \delta(\kappa_1+\kappa_2+\kappa_3\dots-\kappa_k)F_k(\kappa_1,\kappa_2,\kappa_3\dots\kappa_{k-1})\\
&\mathbb{E}[dz(\kappa_1)dz(\kappa_2)\dots dz^*(\kappa_k)] = \delta(\kappa_1+\kappa_2+\kappa_3\dots-\kappa_k)\\
&\quad\times dF_k(\kappa_1,\kappa_2,\kappa_3\dots\kappa_{k-1})
\end{aligned} \tag{9}$$

where $F(\kappa)$ is the spectral distribution function of $z(\kappa)$, $dF(\kappa)$ is the spectral density function, $G(\kappa_1,\kappa_2)$ is the bispectral distribution function, and $dG(\kappa_1,\kappa_2)$ is the bispectral density function. The bispectrum relates to the bispectral density $dG(\kappa_1,\kappa_2)$ through $dG(\kappa_1,\kappa_2) = B(\kappa_1,\kappa_2)d\kappa_1 d\kappa_2$. Finally, $F_k(\kappa_1,\kappa_2,\dots,\kappa_{k-1})$ and $dF_k(\kappa_1,\kappa_2,\dots,\kappa_{k-1})$ are kth-order spectral distribution and density functions, respectively. Generalizing, the kth-order spectral density function relates to the kth-order polyspectrum in Eq. (3) through $dF_k(\kappa_1,\kappa_2,\dots,\kappa_{k-1}) = C_k(\kappa_1,\kappa_2,\dots,\kappa_{k-1})d\kappa_1 d\kappa_2\dots d\kappa_{k-1}$.

Following from this higher-order spectral representation, we are specifically interested in third-order stationary random fields, for which the orthogonality conditions in Eq. (9) hold up to order three. For such random fields, the process is stationary in its first, second, and third order properties (weakly 3rd-order stationary) and can be expressed using the spectral representation in Eq. (8) – referred to herein as the bispectral representation due to the third-order orthogonality and its expression in terms of a stationary bispectrum.

Finally, we are specifically interested in real-valued random fields, for which the Cramer spectral representation can be written as

$$A(x) = \int_{-\infty}^{\infty} \cos(\kappa x)du(\kappa) + sin(\kappa x)dv(\kappa) \tag{10}$$

The components $du(\kappa)$ and $dv(\kappa)$ are the real and imaginary components of the orthogonal increments of $dz(\kappa)$ respectively. Both $du(\kappa)$ and $dv(\kappa)$ possess orthogonal properties similar to $dz(\kappa)$. A detailed description of the orthogonality conditions of these components can be found in [14].

4. Spectral representation methods

Although the general form of the spectral representation was developed by Cramer, Rice [46] was the first to exploit the spectral representation for the purposes of simulation, using its discretized form to simulate one-dimensional, uni-variate Gaussian random processes. Later formalized for second-order multi-dimensional, multi-variate, and non-stationary stochastic processes by Shinozuka [8,9], the method became known as the spectral representation method (SRM). Properties of stochastic processes simulated by the SRM were elaborated in a series of seminal papers on the method by Shinozuka and Deodatis [10,30,31].

Utilizing second-order orthogonal increments $du(\kappa)$ and $dv(\kappa)$ in Eq. (10) gives the following form for the second-order SRM to simulate 1-dimensional, uni-variate random fields:

$$A(x) = \sqrt{2}\sum_{k=0}^{\infty}\sqrt{2S(\kappa_k)\Delta\kappa_k}\cos(\kappa_k x - \phi_k) \tag{11}$$

where $S(\kappa_k)$ is the power spectrum of the process and ϕ_k are independent uniformly distributed random phase angles in the range $[0,2\pi]$. Simulation is then conducted by truncating the summation at an acceptable level, say m terms.

Recently, Shields and Kim [14] extended the SRM for simulation of 3rd-order stationary stochastic processes. Similar to the 2nd-order SRM, incorporating third-order orthogonal increments $du(\kappa)$ and $dv(\kappa)$ in Eq. (10) yields the 3rd-order form of the SRM.

$$\begin{aligned}
A(x) &= \sqrt{2}\sum_{k=0}^{\infty}\sqrt{2S_P(\kappa_k)\Delta\kappa_k}\cos(\kappa_k x - \phi_k)\\
&+ \sqrt{2}\sum_{k=0}^{\infty}\sum_{i+j=k}^{i\geq j\geq 0}\sqrt{2S(\kappa_i+\kappa_j)\Delta(\kappa_i+\kappa_j)}|b_p(\kappa_i,\kappa_j)|\\
&\times\cos\left((\kappa_i+\kappa_j)x - (\phi_i+\phi_j+\beta(\kappa_i,\kappa_j))\right)
\end{aligned} \tag{12}$$

where $b_p(\kappa_i,\kappa_j)$ is the partial bicoherence defined as:

$$b_p^2(\kappa_i,\kappa_j) = \frac{|B(\kappa_i,\kappa_j)|^2}{S_P(\kappa_i)S_P(\kappa_j)S(\kappa_i+\kappa_j)} \tag{13}$$

$S_P(\kappa)$ is the pure power spectrum (i.e. the component of the power spectrum remaining after wave interactions are removed) given by:

$$S_P(\kappa_k) = S(\kappa_k)\left[1 - \sum_{i+j=k}^{i\geq j\geq 0} b_p^2(\kappa_i,\kappa_j)\right] \tag{14}$$

and $\beta(\kappa_i,\kappa_j)$ is the biphase given by:

$$\beta(\kappa_i,\kappa_j) = \arctan\frac{\Im[B(\kappa_i,\kappa_j)]}{\Re[B(\kappa_i,\kappa_j)]} \tag{15}$$

Here, the first term corresponds to the classical 2nd-order SRM on the pure power spectrum and the second term models 3rd-order wave interactions. It has been shown in [14] that simulations generated using Eq. (12), again using a suitable truncation of m terms in the summation, match both the power spectrum and the bispectrum of the random field.

We also note that the 3rd-order expansion presented herein is not necessarily unique. It expresses the higher-order process in terms of random phases. As in the classical 2nd-order SRM, a formulation based on random amplitudes or other alternative orthogonal increments may be possible. Moreover, a direct expansion from the higher-order correlation, akin to the KLE, may be possible. We do not explore these possible alternative formulations.

5. Simulation of multi-dimensional random fields by 3rd-order spectral representation method

The form of the 3rd-order SRM given in Eq. (12) can be used for the simulation of one-dimensional, uni-variate (1D-1V) random fields. In this section, we derive the expression for the simulation of general d-dimensional (dD-1V) third-order random fields. We first derive the simulation formula for 2D random fields as it is the most practical to show and is of particular relevance for many applications. We then extend it for general d-dimensional random fields.

5.1. Simulation of 2-dimensional random fields

Let $A(x_1, x_2)$ be a two-dimensional uni-variate random field with zero mean, 2nd-order autocorrelation function $R_2(\xi_1, \xi_2)$, bispectrum $B(\kappa_{11}, \kappa_{21}, \kappa_{12}, \kappa_{22})$, and 3rd-order autocorrelation function $R_3(\xi_{11}, \xi_{21}, \xi_{12}, \xi_{22})$. Since we are interested in the simulation of real-valued random fields, the power spectrum is symmetric about the origin, i.e. $S(\boldsymbol{\kappa}) = S(-\boldsymbol{\kappa})$, and the following symmetries exist in the bispectrum [14]

$$B(\boldsymbol{\kappa_1}, \boldsymbol{\kappa_2}) = B(\boldsymbol{\kappa_2}, \boldsymbol{\kappa_1}) \tag{16}$$

$$B(\boldsymbol{\kappa_1}, \boldsymbol{\kappa_2}) = B(-\boldsymbol{\kappa_1}, -\boldsymbol{\kappa_2}) \tag{17}$$

$$B(\boldsymbol{\kappa_1}, \boldsymbol{\kappa_2}) = B(-\boldsymbol{\kappa_1} - \boldsymbol{\kappa_2}, \boldsymbol{\kappa_2}) \tag{18}$$

Eqs. (17) and (18) describe two different axes of symmetry along the origin.

Exploiting these symmetries allows us to replace the power spectrum, $S(\kappa_1, \kappa_2)$ defined on the range $(-\infty \le \kappa_1 \le \infty, -\infty \le \kappa_2 \le \infty)$ by $2S(\kappa_1, \kappa_2)$ defined on the range $(0 \le \kappa_1 \le \infty, -\infty \le \kappa_2 \le \infty)$ and replace the bispectrum $B(\kappa_{11}, \kappa_{12}, \kappa_{21}, \kappa_{22})$ defined on the range $(-\infty \le \kappa_{11} \le \infty, -\infty \le \kappa_{21} \le \infty, -\infty \le \kappa_{12} \le \infty, -\infty \le \kappa_{22} \le \infty)$ by $4B(\kappa_{11}, \kappa_{12}, \kappa_{21}, \kappa_{22})$ defined on the range $(0 \le \kappa_{11} \le \infty, 0 \le \kappa_{21} \le \infty, -\infty \le \kappa_{12} \le \infty, -\infty \le \kappa_{22} \le \infty)$.

With these symmetries in place, along with the orthogonality conditions presented in Eq. (9), any real valued 2-dimensional random field $A(x_1, x_2)$ can be expressed in the form

$$A(x_1, x_2) = \int_{-\infty}^{\infty} \int_{0}^{\infty} [\cos(\kappa_1 x_1 + \kappa_2 x_2) du(\kappa_1, \kappa_2) + \sin(\kappa_1 x_1 + \kappa_2 x_2) dv(\kappa_1, \kappa_2)] \tag{19}$$

where processes $u(\kappa_1, \kappa_2)$ and $v(\kappa_1, \kappa_2)$ are defined on the domain $0 < \kappa_1 < \infty, -\infty < \kappa_2 < \infty$ and obey the following the orthogonality conditions [47]:

$$\mathbb{E}[u(\kappa_1, \kappa_2)] = \mathbb{E}[v(\kappa_1, \kappa_2)] = 0 \tag{20}$$

$$\mathbb{E}[du(\kappa_1, \kappa_2)] = \mathbb{E}[dv(\kappa_1, \kappa_2)] = 0 \tag{21}$$

$$\begin{aligned}
&\mathbb{E}[u^2(\kappa_1, \kappa_2)] = \mathbb{E}[v^2(\kappa_1, \kappa_2)] = F_1(\kappa_1, \kappa_2) \\
&\mathbb{E}[u(\kappa_{11}, \kappa_{21}) u(\kappa_{12}, \kappa_{22}) u(\kappa_{11} + \kappa_{12}, \kappa_{21} + \kappa_{22})] = \\
&\mathbb{E}[v(\kappa_{11}, \kappa_{21}) v(\kappa_{12}, \kappa_{22}) v(\kappa_{11} + \kappa_{12}, \kappa_{21} + \kappa_{22})] = G_1(\kappa_{11}, \kappa_{21}, \kappa_{12}, \kappa_{22}) \\
&\mathbb{E}[u(\kappa_1, \kappa_2) v(\kappa_1', \kappa_2')] = 0 \\
&\mathbb{E}[u(\kappa_1, \kappa_2) v(\kappa_1', \kappa_2') v(\kappa_1'', \kappa_2'')] = 0 \\
&\mathbb{E}[u(\kappa_1, \kappa_2) u(\kappa_1', \kappa_2') v(\kappa_1'', \kappa_2'')] = 0
\end{aligned} \tag{22}$$

$$\begin{aligned}
&\mathbb{E}[du^2(\kappa_1, \kappa_2)] = \mathbb{E}[dv^2(\kappa_1, \kappa_2)] = S_1(\kappa_1, \kappa_2) d\kappa_1 d\kappa_2 \\
&\mathbb{E}[du(\kappa_1, \kappa_2) du(\kappa_1', \kappa_2')] = 0 \; if \; \kappa_1 \neq \kappa_1' \; or \; \kappa_2 \neq \kappa_2' \\
&\mathbb{E}[dv(\kappa_1, \kappa_2) dv(\kappa_1', \kappa_2')] = 0 \; if \; \kappa_1 \neq \kappa_1' \; or \; \kappa_2 \neq \kappa_2' \\
&\mathbb{E}[du(\kappa_1, \kappa_2) dv(\kappa_1', \kappa_2')] = 0
\end{aligned} \tag{23}$$

$$\begin{aligned}
&\mathbb{E}[du(\kappa_1, \kappa_2) du(\kappa_1', \kappa_2') du(\kappa_1'', \kappa_2'')] = 2\Re B(\kappa_1', \kappa_1'', \kappa_2', \kappa_2'') \\
&\mathbb{E}[du(\kappa_1, \kappa_2) du(\kappa_1', \kappa_2') dv(\kappa_1'', \kappa_2'')] = -2\Im B(\kappa_1', \kappa_1'', \kappa_2', \kappa_2'') \\
&\mathbb{E}[du(\kappa_1, \kappa_2) dv(\kappa_1', \kappa_2') du(\kappa_1'', \kappa_2'')] = -2\Im B(\kappa_1', \kappa_1'', \kappa_2', \kappa_2'') \\
&\mathbb{E}[du(\kappa_1, \kappa_2) dv(\kappa_1', \kappa_2') dv(\kappa_1'', \kappa_2'')] = -2\Re B(\kappa_1', \kappa_1'', \kappa_2', \kappa_2'') \\
&\mathbb{E}[dv(\kappa_1, \kappa_2) du(\kappa_1', \kappa_2') du(\kappa_1'', \kappa_2'')] = 2\Im B(\kappa_1', \kappa_1'', \kappa_2', \kappa_2'') \\
&\mathbb{E}[dv(\kappa_1, \kappa_2) du(\kappa_1', \kappa_2') dv(\kappa_1'', \kappa_2'')] = 2\Re B(\kappa_1', \kappa_1'', \kappa_2', \kappa_2'') \\
&\mathbb{E}[dv(\kappa_1, \kappa_2) dv(\kappa_1', \kappa_2') du(\kappa_1'', \kappa_2'')] = 2\Re B(\kappa_1', \kappa_1'', \kappa_2', \kappa_2'') \\
&\mathbb{E}[dv(\kappa_1, \kappa_2) dv(\kappa_1', \kappa_2') dv(\kappa_1'', \kappa_2'')] = -2\Im B(\kappa_1', \kappa_1'', \kappa_2', \kappa_2'') \\
&\text{if } \kappa_1 = \kappa_1' + \kappa_1'' \\
&\text{otherwise } 0
\end{aligned} \tag{24}$$

where $\Re$ and $\Im$ denote the real and imaginary components respectively. It can be seen in [44] that Eq. (19) does, indeed represent a stochastic field with zero mean and 2nd-order and 3rd-order autocorrelation functions $R_2(\xi_1, \xi_2)$ and $R_3(\xi_{11}, \xi_{21}, \xi_{12}, \xi_{22})$, respectively.

Discretizing Eq. (19), gives

$$\begin{aligned}
A(x_1, x_2) = \sum_{n_2=-\infty}^{\infty} \sum_{n_1=0}^{\infty} [&\cos(\kappa_{1n_1} x_1 + \kappa_{2n_2} x_2) du(\kappa_{1n_1}, \kappa_{2n_2}) \\
&+ \sin(\kappa_{1n_1} x_1 + \kappa_{2n_2} x_2) dv(\kappa_{1n_1}, \kappa_{2n_2})]
\end{aligned} \tag{25}$$

where $\kappa_{1n_1} = n_1 \Delta\kappa_1$ and $\kappa_{2n_2} = n_2 \Delta\kappa_2$, with sufficiently small finite $\Delta\kappa_1$ and $\Delta\kappa_2$. If $du(\kappa_{1n_1}, \kappa_{2n_2})$ and $dv(\kappa_{1n_1}, \kappa_{2n_2})$ are defined as

$$\begin{aligned}
du(\kappa_{1n_1}, \kappa_{2n_2}) = &\sqrt{2} A_{pn_1n_2} \cos \boldsymbol{\Phi}_{n_1n_2} \\
&+ \sum_{i_1+j_1=n_1}^{i_1 \ge j_1 \ge 0} \sum_{i_2+j_2=n_2}^{|n_2| \ge |i_2| \ge |j_2| \ge 0} \sqrt{2} A_{n_1n_2} b_p(\kappa_{1i_1}, \kappa_{1j_1}, \kappa_{2i_2}, \kappa_{2j_2}) \\
&\times \cos(\boldsymbol{\Phi}_{i_1i_2} + \boldsymbol{\Phi}_{j_1j_2} + \beta(\kappa_{1i_1}, \kappa_{1j_1}, \kappa_{2i_2}, \kappa_{2j_2}))
\end{aligned} \tag{26}$$

$$\begin{aligned}
dv(\kappa_{1n_1}, \kappa_{2n_2}) = &-\sqrt{2} A_{pn_1n_2} \sin \boldsymbol{\Phi}_{n_1n_2} \\
&- \sum_{i_1+j_1=n_1}^{i_1 \ge j_1 \ge 0} \sum_{i_2+j_2=n_2}^{|n_2| \ge |i_2| \ge |j_2| \ge 0} \sqrt{2} A_{n_1n_2} b_p(\kappa_{1i_1}, \kappa_{1j_1}, \kappa_{2i_2}, \kappa_{2j_2}) \\
&\times \sin(\boldsymbol{\Phi}_{i_1i_2} + \boldsymbol{\Phi}_{j_1j_2} + \beta(\kappa_{1i_1}, \kappa_{1j_1}, \kappa_{2i_2}, \kappa_{2j_2}))
\end{aligned} \tag{27}$$

where

$$A_{pn_1n_2} = \sqrt{2 S_p(\kappa_{1n_1}, \kappa_{2n_2}) \Delta\kappa_1 \Delta\kappa_2} \tag{28}$$

$$A_{n_1n_2} = \sqrt{2 S(\kappa_{1n_1}, \kappa_{2n_2}) \Delta\kappa_1 \Delta\kappa_2} \tag{29}$$

$$S_p(\kappa_{1n_1}, \kappa_{2n_2}) = S(\kappa_{1n_1}, \kappa_{2n_2}) \Big(1 - \sum_{i_1+j_1=n_1}^{i_1 \ge j_1 \ge 0} \sum_{i_2+j_2=n_2}^{|n_2| \ge |i_2| \ge |j_2| \ge 0} b_p^2(\kappa_{1i_1}, \kappa_{1j_1}, \kappa_{2i_2}, \kappa_{2j_2})\Big) \tag{30}$$

$$b_p^2(\kappa_{1i_1}, \kappa_{1j_1}, \kappa_{2i_2}, \kappa_{2j_2}) = \frac{|B(\kappa_{1i_1}, \kappa_{1j_1}, \kappa_{2i_2}, \kappa_{2j_2})|^2 \Delta\kappa_1 \Delta\kappa_2}{S_p(\kappa_{1i_1}, \kappa_{2i_2}) S_p(\kappa_{1j_1}, \kappa_{2j_2}) S(\kappa_{1(i_1+j_1)}, \kappa_{2(i_2+j_2)})} \tag{31}$$

and $\boldsymbol{\Phi}_{n_1n_2}$ are independent random phase angles uniformly distributed in the range $[0, 2\pi]$, then the resulting 2-dimensional random field is third-order stationary possessing power spectrum $S(\kappa_1, \kappa_2)$ and bispectrum $B(\kappa_{11}, \kappa_{12}, \kappa_{21}, \kappa_{22})$. It is proven in [44] that the orthogonality requirements on $du(\kappa_{1n_1}, \kappa_{2n_2})$ and $dv(\kappa_{1n_1}, \kappa_{2n_2})$ are satisfied, and therefore that the process is third-order stationary possessing the prescribed spectra.

Using the above proposed increments, the following series representation is obtained

$$A(x_1,x_2)=\sum_{n_2=-\infty}^{\infty}\sum_{n_1=0}^{\infty}\Big[\sqrt{2}A_{pn_1n_2}\cos(\kappa_{1n_1}x_1+\kappa_{2n_2}x_2+\Phi_{n_1n_2})+\sum_{i_1+j_1=n_1}^{i_1\geq j_1\geq 0}\sum_{i_2+j_2=n_2}^{|n_2|\geq|i_2|\geq|j_2|\geq 0}\sqrt{2}A_{n_1n_2}b_p(\kappa_{1i_1},\kappa_{1j_1},\kappa_{2i_2},\kappa_{2j_2})\cos(\kappa_{1n_1}x_1+\kappa_{2n_2}x_2+\Phi_{i_1i_2}+\Phi_{j_1j_2}+\beta(\kappa_{1i_1},\kappa_{1j_1},\kappa_{2i_2},\kappa_{2j_2}))\Big] \tag{32}$$

By rearranging the terms, we can express the series over only positive indices as

$$\begin{aligned}A(x_1,x_2)=\sqrt{2}\sum_{n_2=0}^{\infty}\sum_{n_1=0}^{\infty}\Big[&\sqrt{S_p(\kappa_{1n_1},\kappa_{2n_2})\Delta\kappa_1\Delta\kappa_2}\cos(\kappa_{1n_1}x_1+\kappa_{2n_2}x_2+\Phi^{(1)}_{n_1n_2})\\&+\sqrt{S_p(\kappa_{n_1},-\kappa_{n_2})\Delta\kappa_1\Delta\kappa_2}\cos(\kappa_{1n_1}x_1-\kappa_{2n_2}x_2+\Phi^{(2)}_{n_1n_2})\\&+\sum_{i_1+j_1=n_1}^{i_1\geq j_1\geq 0}\sum_{i_2+j_2=n_2}^{i_2\geq j_2\geq 0}\sqrt{2S(\kappa_{1n_1},\kappa_{2n_2})}b_p(\kappa_{1i_1},\kappa_{1j_1},\kappa_{2i_2},\kappa_{2j_2})\\&\cos(\kappa_{1n_1}x_1+\kappa_{2n_2}x_2+\Phi^{(1)}_{i_1i_2}+\Phi^{(1)}_{j_1j_2}+\beta(\kappa_{1i_1},\kappa_{1j_1},\kappa_{2i_2},\kappa_{2j_2}))\\&+\sum_{i_1+j_1=n_1}^{i_1\geq j_1\geq 0}\sum_{i_2+j_2=n_2}^{i_2\geq j_2\geq 0}\sqrt{2S(\kappa_{1n_1},-\kappa_{2n_2})}b_p(\kappa_{1i_1},\kappa_{1j_1},-\kappa_{2i_2},-\kappa_{2j_2})\\&\cos(\kappa_{1n_1}x_1-\kappa_{2n_2}x_2+\Phi^{(2)}_{i_1i_2}+\Phi^{(2)}_{j_1j_2}+\beta(\kappa_{1i_1},\kappa_{1j_1},-\kappa_{2i_2},-\kappa_{2j_2}))\\&+\sum_{i_1+j_1=n_1}^{i_1\geq j_1\geq 0}\sum_{i_2+j_2=n_2}^{i_2\geq j_2\geq 0}\sqrt{2S(\kappa_{1n_1},-\kappa_{2i_2}+\kappa_{2j_2})}b_p(\kappa_{1i_1},\kappa_{1j_1},-\kappa_{2i_2},\kappa_{2j_2})\\&\cos(\kappa_{1n_1}x_1-\kappa_{2i_2}x_2+\kappa_{2j_2}x_2+\Phi^{(2)}_{i_1i_2}+\Phi^{(1)}_{j_1j_2}+\beta(\kappa_{1i_1},\kappa_{1j_1},-\kappa_{2i_2},\kappa_{2j_2}))\\&+\sum_{i_1+j_1=n_1}^{i_1\geq j_1\geq 0}\sum_{i_2+j_2=n_2}^{i_2\geq j_2\geq 0}\sqrt{2S(\kappa_{1n_1},+\kappa_{2i_2}-\kappa_{2j_2})}b_p(\kappa_{1i_1},\kappa_{1j_1},\kappa_{2i_2},-\kappa_{2j_2})\\&\cos(\kappa_{1n_1}x_1+\kappa_{2i_2}x_2-\kappa_{2j_2}x_2+\Phi^{(1)}_{i_1i_2}+\Phi^{(2)}_{j_1j_2}+\beta(\kappa_{1i_1},\kappa_{1j_1},\kappa_{2i_2},-\kappa_{2j_2}))\Big]\end{aligned} \tag{33}$$

While Eq. (32) provides a compact notation, Eq. (33) sums only over positive indices which may be beneficial for practical implementation. Note that, since the formula sums over the positive and negative range of κ_2 simultaneously, we need to use two different sets of random phase angles which are differentiated using superscripts $\Phi^{(1)}$ and $\Phi^{(2)}$.

While Eqs. (32)–(33) provide a theoretical framework for the simulation of 2-dimensional third-order stationary random fields, the infinite series representation of Eq. (32) cannot be implemented in practice. A practical implementation truncates these summations as

$$A(x_1,x_2)=\sum_{n_2=-N_2}^{N_2}\sum_{n_1=0}^{N_1}\Big[\sqrt{2}A_{pn_1n_2}\cos(\kappa_{1n_1}x_1+\kappa_{2n_2}x_2+\Phi_{n_1n_2})+\sum_{i_1+j_1=n_1}^{i_1\geq j_1\geq 0}\sum_{i_2+j_2=n_2}^{|n_2|\geq|i_2|\geq|j_2|\geq 0}\sqrt{2}A_{n_1n_2}b_p(\kappa_{1i_1},\kappa_{1j_1},\kappa_{2i_2},\kappa_{2j_2})\cos(\kappa_{1n_1}x_1+\kappa_{2n_2}x_2+\Phi_{i_1i_2}+\Phi_{j_1j_2}+\beta(\kappa_{1i_1},\kappa_{1j_1},\kappa_{2i_2},\kappa_{2j_2}))\Big] \tag{34}$$

where the various terms are defined as in Eqs. (28)–(31), $\Delta\kappa_1=\frac{\kappa_{1u}}{N_1}$ and $\Delta\kappa_2=\frac{\kappa_{2u}}{N_2}$ are the cutoff wave-numbers for the x_1 and x_2 axes respectively, and

$$S(\kappa_1,0)=S(0,\kappa_2)=0 \text{ for } -\infty\leq\kappa_1\leq\infty \text{ and } -\infty\leq\kappa_2\leq\infty \tag{35}$$

$$\begin{aligned}&B(\kappa_{11},\kappa_{12},\kappa_{21},0)=B(\kappa_{11},\kappa_{12},0,\kappa_{22})=B(\kappa_{11},0,\kappa_{21},\kappa_{22})\\&=B(0,\kappa_{12},\kappa_{21},\kappa_{22})=0\\&\text{for } -\infty\leq\kappa_{11}\leq\infty\ ;-\infty\leq\kappa_{12}\leq\infty \text{ and } -\infty\leq\kappa_{21}\leq\infty;-\infty\leq\kappa_{22}\leq\infty\end{aligned} \tag{36}$$

The cutoff wave-numbers are chosen to satisfy the conditions

$$\int_0^{\kappa_{1u}}\int_{-\kappa_{2u}}^{\kappa_{2u}}S(\kappa_1,\kappa_2)d\kappa_1d\kappa_2=(1-\epsilon)\int_0^{\infty}\int_{-\infty}^{\infty}S(\kappa_1,\kappa_2)d\kappa_1d\kappa_2 \tag{37}$$

and

$$\begin{aligned}&\int_0^{\kappa_{1u}}\int_0^{\kappa_{1u}}\int_{-\kappa_{2u}}^{\kappa_{2u}}\int_{-\kappa_{2u}}^{\kappa_{2u}}B(\kappa_{11},\kappa_{12},\kappa_{21},\kappa_{22})d\kappa_{11}d\kappa_{12}d\kappa_{21}d\kappa_{22}\\&=(1-\epsilon)\int_0^{\kappa_{1u}}\int_0^{\kappa_{1u}}\int_{-\kappa_{2u}}^{\kappa_{2u}}\int_{-\kappa_{2u}}^{\kappa_{2u}}B(\kappa_{11},\kappa_{12},\kappa_{21},\kappa_{22})d\kappa_{11}d\kappa_{12}d\kappa_{21}d\kappa_{22}\end{aligned} \tag{38}$$

where $\epsilon\ll 1$. This effectively means that the power spectrum and the bispectrum above the cutoff wave-numbers are mathematically or physically insignificant.

It is straightforward to show that the simulated random fields are periodic along the x_1 and x_2 axes with periods $L_{x_1}=\frac{2\pi}{\Delta\kappa_1}$ and $L_{x_2}=\frac{2\pi}{\Delta\kappa_2}$. Additionally, the conditions $\Delta x_1\leq\frac{2\pi}{2\kappa_{1u}}$ and $\Delta x_2\leq\frac{2\pi}{2\kappa_{2u}}$ are imposed on the spatial increments to prevent aliasing. Lastly, given the finite truncation of the summations, the values of the field in this expansion $A(x_1,x_2)$ are theoretically bounded within the range

$$\begin{aligned}&\Big[-\sum_{n_2=-N_2}^{N_2}\sum_{n_1=0}^{N_1}[\sqrt{2}A_{pn_1n_2}-\sum_{i_1+j_1=n_1}^{i_1\geq j_1\geq 0}\sum_{i_2+j_2=n_2}^{|n_2|\geq|i_2|\geq|j_2|\geq 0}\sqrt{2}A_{n_1n_2}b_p(\kappa_{1i_1},\kappa_{1j_1},\kappa_{2i_2},\kappa_{2j_2})],\\&\sum_{n_2=-N_2}^{N_2}\sum_{n_1=0}^{N_1}[\sqrt{2}A_{pn_1n_2}+\sum_{i_1+j_1=n_1}^{i_1\geq j_1\geq 0}\sum_{i_2+j_2=n_2}^{|n_2|\geq|i_2|\geq|j_2|\geq 0}\sqrt{2}A_{n_1n_2}b_p(\kappa_{1i_1},\kappa_{1j_1},\kappa_{2i_2},\kappa_{2j_2})]\Big]\end{aligned} \tag{39}$$

5.2. Simulation of d-dimensional random fields

Let $A(x_1,x_2,\dots,x_d)$ be a d-dimensional uni-variate (dD-1V) third-order stationary random field with zero mean, power spectrum $S(\kappa_1,\kappa_2,\dots,\kappa_d)$, 2nd-order autocorrelation function $R_2(\xi_1,\xi_2,\dots,\xi_d)$, bispectrum $B(\kappa_{11},\kappa_{12},\kappa_{21},\kappa_{22},\kappa_{31},\kappa_{32},\dots,\dots,\kappa_{n1},\kappa_{n2})$, and 3rd-order autocorrelation function $R_3(\xi_{11},\xi_{12},\xi_{21},\xi_{22},\xi_{31},\xi_{32},\dots,\dots,\xi_{n1},\xi_{n2})$. For convenience, let us define the following new vector quantities:

Position vector: $\overline{x}=[x_1,x_2,\dots,x_n]^T$

Separation vector: $\overline{\xi}=[\xi_1,\xi_2,\dots,\xi_n]^T$

Wave number vector: $\overline{\kappa}=[\kappa_1,\kappa_2,\dots,\kappa_n]^T$

The symmetries in Eqs. (16)–(18) still hold.

The formula for the simulation of general d-dimensional random fields follows closely from the 2D case as

$$\begin{aligned}A(\overline{x})=\sum_{n_d=-N_d}^{N_d}\cdots\sum_{n_2=-N_2}^{N_2}\sum_{n_1=0}^{N_1}&[\sqrt{2}A_{p\overline{n}}\cos(\overline{\kappa}\cdot\overline{x}+\Phi_{\overline{n}})\\&+\sum_{i_1+j_1=n_1}^{i_1\geq j_1\geq 0}\sum_{i_2+j_2=n_2}^{|n_2|\geq|i_2|\geq|j_2|\geq 0}\cdots\sum_{i_d+j_d=n_d}^{|n_d|\geq|i_d|\geq|j_d|\geq 0}\sqrt{2}A_{\overline{n}}b_p(\overline{\kappa}_{\overline{i}},\overline{\kappa}_{\overline{j}})\\&\times\cos(\overline{\kappa}\cdot\overline{x}+\Phi_{\overline{i}}+\Phi_{\overline{j}}+\beta(\overline{\kappa}_{\overline{i}},\overline{\kappa}_{\overline{j}}))]\end{aligned} \tag{40}$$

where

$$\begin{aligned}&A_{p\overline{n}}=\sqrt{2S_p(\overline{\kappa}_{\overline{n}})\Delta\kappa_1\Delta\kappa_2\dots\Delta\kappa_d},\ A_{\overline{n}}=\sqrt{2S(\overline{\kappa}_{\overline{n}})\Delta\kappa_1\Delta\kappa_2\dots\Delta\kappa_d}\\&S_p(\overline{\kappa}_{\overline{n}})=S(\overline{\kappa}_{\overline{n}})\Big(1-\sum_{i_1+j_1=n_1}^{i_1\geq j_1\geq 0}\sum_{i_2+j_2=n_2}^{|n_1|\geq|i_1|\geq|j_1|\geq 0}\cdots\sum_{i_d+j_d=n_d}^{|n_d|\geq|i_d|\geq|j_d|\geq 0}b_p^2(\overline{\kappa}_i,\overline{\kappa}_j)\Big)\\&b_p^2(\overline{\kappa}_{\overline{i}},\overline{\kappa}_{\overline{j}})=\frac{|B(\overline{\kappa}_{\overline{i}},\overline{\kappa}_{\overline{j}})|^2\Delta\kappa_1\Delta\kappa_2\dots\Delta\kappa_d}{S_p(\overline{\kappa}_{\overline{i}})S_p(\overline{\kappa}_{\overline{j}})S(\overline{\kappa}_{\overline{n}})}\\&\kappa_{1n_1}=n_1\Delta\kappa_1\ ;\ \kappa_{2n_2}=n_2\Delta\kappa_2;\dots;\kappa_{dn_d}=n_d\Delta\kappa_d\\&\Delta\kappa_1=\frac{\kappa_{1u}}{N_1}\ ;\ \Delta\kappa_2=\frac{\kappa_{2u}}{N_2};\dots;\Delta\kappa_d=\frac{\kappa_{du}}{N_d}\end{aligned} \tag{41}$$

and

$$\begin{aligned}&S(0,\kappa_2,\dots,\kappa_d)=S(\kappa_1,0,\dots,\kappa_d)=S(\kappa_1,\kappa_2,\dots,0)=0\\&\text{for } -\infty\leq\kappa_1\leq\infty\ -\infty\leq\kappa_2\leq\infty;\dots;-\infty\leq\kappa_d\leq\infty\end{aligned} \tag{42}$$

$$B(0,\kappa_{12},\dots\kappa_{d1},\kappa_{d2}) = B(\kappa_{11},0,\dots\kappa_{d1},\kappa_{d2}) = \cdots = B(\kappa_{11},\kappa_{12},\dots 0,\kappa_{d2}) = B(\kappa_{11},\kappa_{12},\dots\kappa_{d1},0) = 0 \quad \text{for } -\infty \le \kappa_{11} \le \infty\ ; -\infty \le \kappa_{12} \le \infty; \dots; -\infty \le \kappa_{d1} \le \infty; -\infty \le \kappa_{d2} \le \infty \tag{43}$$

In the above expressions, the overline subscripts denote the iterable index sets $\overline{n} = \{n_1, n_2, \dots, n_d\}$, $\overline{i} = \{i_1, i_2, \dots, i_d\}$, and $\overline{j} = \{j_1, j_2, \dots, j_d\}$. In particular, $\Phi_{\overline{n}}$ denotes the dth-order tensor of random phase angles indexed as $\Phi_{n_1 n_2 \dots n_d}$ and $A_{p\overline{n}}$, $A_{\overline{n}}$ denote dth-order tensors of amplitudes having components $A_{pn_1 n_2 \dots n_d}$, $A_{n_1 n_2 \dots n_d}$. Indexing of the wave number combines the vector overline notations with the overline subscripts such that $\overline{\kappa}_{\overline{n}}$ denotes the wave number set $(\kappa_{1n_1}, \kappa_{2n_2}, \dots, \kappa_{dn_d})$. Finally, κ_{1u}, κ_{2u}, ...and κ_{du} are the cutoff wave-numbers for the x_1, x_2 ... x_d axes respectively, satisfying

$$\int_{-\overline{\kappa}_u}^{\overline{\kappa}_u} S(\overline{\kappa})d\overline{\kappa} = (1-\epsilon)\int_{-\infty}^{\infty} S(\overline{\kappa})d\overline{\kappa} \tag{44}$$

$$\int_{-\overline{\kappa}_{\overline{i}u}}^{\overline{\kappa}_{\overline{i}u}}\int_{-\overline{\kappa}_{\overline{j}u}}^{\overline{\kappa}_{\overline{j}u}} B(\overline{\kappa}_{\overline{i}},\overline{\kappa}_{\overline{j}})d\overline{\kappa}_{\overline{i}}d\overline{\kappa}_{\overline{j}} = (1-\epsilon)\int_{-\infty}^{\infty}\int_{-\infty}^{\infty} B(\overline{\kappa}_{\overline{i}},\overline{\kappa}_{\overline{j}})d\overline{\kappa}_{\overline{i}}d\overline{\kappa}_{\overline{j}} \tag{45}$$

where $\epsilon \ll 1$.

The simulated random fields are periodic along the x_1, x_2 ... x_d with period

$$L_{x_1} = \frac{2\pi}{\Delta\kappa_1}, \quad L_{x_2} = \frac{2\pi}{\Delta\kappa_2}, \quad \dots, \quad L_{x_d} = \frac{2\pi}{\Delta\kappa_d} \tag{46}$$

and the conditions to prevent aliasing are given as

$$\Delta x_1 \le \frac{2\pi}{2\kappa_{1u}}, \quad \Delta x_2 \le \frac{2\pi}{2\kappa_{2u}}, \quad \dots, \Delta x_d \le \frac{2\pi}{2\kappa_{du}} \tag{47}$$

5.3. Simulation of quadrant random fields

Quadrant random fields have additional symmetries beyond those presented above. Specifically, in 2D they are given by

$$S(\kappa_1,\kappa_2) = S(I_1\kappa_1, I_2\kappa_2) \text{ for } I_1, I_2 = \pm 1$$
$$B(\kappa_{11},\kappa_{12},\kappa_{21},\kappa_{22}) = B(I_{11}\kappa_{11}, I_{12}\kappa_{12}, I_{21}\kappa_{21}, I_{22}\kappa_{22}) \quad \text{for } I_{11}, I_{12}, I_{21}, I_{22} = \pm 1 \tag{48}$$

As a result of these additional symmetries, the simulation formula for 2D-1V third-order quadrant random fields simplifies to

$$\begin{aligned} A(x_1,x_2) = \sqrt{2}\sum_{n_2=0}^{N_2}\sum_{n_1=0}^{N_1}\sqrt{S_p(\kappa_{1n_1},\kappa_{2n_2})\Delta\kappa_1\Delta\kappa_2}\Big[& \cos(\kappa_{1n_1}x_1 + \kappa_{2n_2}x_2 + \Phi^{(1)}_{n_1n_2}) \\ & + \cos(\kappa_{1n_1}x_1 - \kappa_{2n_2}x_2 + \Phi^{(2)}_{n_1n_2}) \\ & + \sqrt{2}\sum_{i_1+j_1=n_1}^{i_1\ge j_1\ge 0}\sum_{i_2+j_2=n_2}^{i_2\ge j_2\ge 0}\sqrt{S(\kappa_{1n_1},\kappa_{2n_2})}b_p(\kappa_{1i_1},\kappa_{1j_1},\kappa_{2i_2},\kappa_{2j_2}) \\ & \Big[\cos(\kappa_{1n_1}x_1 + \kappa_{2n_2}x_2 + \Phi^{(1)}_{i_1i_2} + \Phi^{(1)}_{j_1j_2} + \beta(\kappa_{1i_1},\kappa_{1j_1},\kappa_{2i_2},\kappa_{2j_2})) \\ & + \cos(\kappa_{1n_1}x_1 - \kappa_{2n_2}x_2 + \Phi^{(2)}_{i_1i_2} + \Phi^{(2)}_{j_1j_2} + \beta(\kappa_{1i_1},\kappa_{1j_1},-\kappa_{2i_2},-\kappa_{2j_2})) \\ & + \cos(\kappa_{1n_1}x_1 - \kappa_{2i_2}x_2 + \kappa_{2j_2}x_2 + \Phi^{(2)}_{i_1i_2} + \Phi^{(1)}_{j_1j_2} + \beta(\kappa_{1i_1},\kappa_{1j_1},-\kappa_{2i_2},\kappa_{2j_2})) \\ & + \cos(\kappa_{1n_1}x_1 + \kappa_{2i_2}x_2 - \kappa_{2j_2}x_2 + \Phi^{(1)}_{i_1i_2} + \Phi^{(2)}_{j_1j_2} + \beta(\kappa_{1i_1},\kappa_{1j_1},\kappa_{2i_2},\kappa_{2j_2}))\Big]\Big] \end{aligned} \tag{49}$$

where the various terms are defined as before.

The symmetries in the d-dimensional polyspectra for quadrant random fields are given by

$$S(\kappa_1,\kappa_2,\dots,\kappa_d) = S(I_1\kappa_1, I_2\kappa_2, \dots, I_d\kappa_d) \text{ for } I_1, I_2, \dots I_d = \pm 1$$
$$B(\kappa_{11},\kappa_{12},\kappa_{21},\kappa_{22},\dots,\dots,\kappa_{d1},\kappa_{d2}) = B(I_{11}\kappa_{11}, I_{12}\kappa_{12}, I_{21}\kappa_{21}, I_{22}\kappa_{22},\dots,\dots,I_{d1}\kappa_{d1}, I_{d2}\kappa_{d2}) \quad \text{for } I_{11}, I_{12}, I_{21}, I_{22},\dots,\dots,I_{d1}, I_{d2} = \pm 1 \tag{50}$$

As a result, the simulation formula for dD-1V third-order quadrant random fields simplifies to

$$\begin{aligned} A(x_1,x_2,\dots,x_d) = \sqrt{2}\sum_{n_d=0}^{N_d}\cdots\sum_{n_2=0}^{N_2}\sum_{n_1=0}^{N_1}\Bigg[& \sqrt{S_p(\kappa_{1n_1},\kappa_{2n_2},\dots,\kappa_{dn_d})\Delta\kappa_1\Delta\kappa_2\dots\Delta\kappa_d} \\ & \sum_{I_1=1,I_2=\pm1,\dots,I_d=\pm1}\cos(I_1\kappa_{1n_1}x_1 + I_2\kappa_{2n_2}x_2 + \cdots + I_d\kappa_{dn_d}x_3 + \Phi^{I_1I_2\dots I_d}_{n_1n_2\dots n_d}) \\ & + \sqrt{2}\sum_{i_1+j_1=n_1}^{i_1\ge j_1\ge 0}\sum_{i_2+j_2=n_2}^{i_2\ge j_2\ge 0}\cdots\sum_{i_d+j_d=n_d}^{i_d\ge j_d\ge 0}\sqrt{S(\kappa_{1n_1},\kappa_{2n_2},\dots,\kappa_{dn_d})} \\ & \times b_p(\kappa_{1i_1},\kappa_{1j_1},\kappa_{2i_2},\kappa_{2j_2},\dots,\kappa_{di_d},\kappa_{dj_d}) \\ & \Bigg[\sum_{I_1=1,I_{21}=\pm1,I_{22}=\pm1,\dots I_{d1}=\pm1,I_{d2}=\pm1}\cos\big(I_1\kappa_{1i_1}x_1 + I_{21}\kappa_{2i_2}x_2 + I_{22}\kappa_{2j_2}x_2 + \cdots \\ & + I_{d1}\kappa_{di_d}x_d + I_{d2}\kappa_{dj_d}x_d + \Phi^{I_1I_{21}\dots I_{d1}}_{i_1i_2\dots i_d} + \Phi^{I_1I_{22}\dots I_{d2}}_{j_1j_2\dots j_d} \\ & + \beta(\kappa_{1i_1},\kappa_{1j_1},\kappa_{2i_2},\kappa_{2j_2},\dots,\kappa_{di_d},\kappa_{dj_d})\big)\Bigg]\Bigg] \end{aligned} \tag{51}$$

where

$$S_p(\kappa_{1n_1},\kappa_{2n_2},\dots\kappa_{dn_d}) = S(\kappa_{1n_1},\kappa_{2n_2},\dots,\kappa_{dn_d})\Bigg(1 - \sum_{i_1+j_1=n_1}^{i_1\ge j_1\ge 0}\sum_{i_2+j_2=n_2}^{i_2\ge j_2\ge 0}\cdots\sum_{i_d+j_d=n_d}^{i_d\ge j_d\ge 0} b_p^2(\kappa_{1i_1},\kappa_{1j_1},\kappa_{2i_2},\kappa_{2j_2},\dots,\kappa_{di_d},\kappa_{dj_d})\Bigg)$$
$$b_p^2(\kappa_{1i_1},\kappa_{1j_1},\kappa_{2i_2},\kappa_{2j_2},\dots,\kappa_{di_d},\kappa_{dj_d}) = \frac{|B(\kappa_{1i_1},\kappa_{1j_1},\kappa_{2i_1},\kappa_{2j_2},\dots,\kappa_{di_d},\kappa_{dj_d})|^2\Delta\kappa_1\Delta\kappa_2\dots\Delta\kappa_d}{S_p(\kappa_{1i_1},\kappa_{2i_2},\dots,\kappa_{di_d})S_p(\kappa_{1j_1},\kappa_{2j_2},\dots,\kappa_{dj_d})S(\kappa_{1(i_1+j_1)},\kappa_{2(i_2+j_2)},\dots,\kappa_{d(i_d+j_d)})} \tag{52}$$

Note that we forego the overline index set notation in lieu of the full indicial notation given the introduction of additional summations associated with the symmetries. For simulation purposes, we further note that the quadrant random fields require the generation of 2^d sets of dth-order tensors of random phase angles.

5.4. Simulation of one-dimensional random fields with FFT

The simulation formulae presented up until now can be used for simulating random fields, but they grow increasingly computational intensive with increasing dimension; so much so that simulating 3-dimensional random fields becomes impractical. Assuming that all required data such as partial bicoherences, biphase angles, etc. have been computed a priori, sample function generation for a 1D-1V process using the truncated form of Eq. (12) has complexity $O(MN)$. This complexity increases exponentially for multi-dimensional random fields to order $O((MN)^d)$ where d is the dimension of the random field. Here, we introduce a fast Fourier transform (FFT) based implementation to reduce the complexity of the simulations.

We first develop an FFT based implementation for simulation of 1D-1V third-order random fields and subsequently extend it to the 2D-1V and dD-1V cases. Let us start by writing Eq. (12) in its complete discretized form as

$$\begin{aligned} A(m\Delta x) = & \sqrt{2}\sum_{n=0}^{\infty}\sqrt{2S(k\Delta\kappa)\Delta\kappa(1 - \sum_{i+j=n}^{i\ge j\ge 0} b_p^2(\kappa_i,\kappa_j))}\cos\big((n\Delta\kappa)(m\Delta x) - \phi_k\big) \\ & + \sqrt{2}\sum_{n=0}^{\infty}\sum_{i+j=n}^{i\ge j\ge 0}\sqrt{2S(n\Delta\kappa)\Delta\kappa}|b_p(\kappa_i,\kappa_j)| \\ & \times\cos\big((n\Delta\kappa)(m\Delta x) - (\phi_i + \phi_j + \beta(\kappa_i,\kappa_j))\big) \end{aligned} \tag{53}$$

Simplifying the representation from two additive terms to only one term we get

$$A(m\Delta x) = \sqrt{2}\sum_{n=0}^{\infty}\sqrt{2S(n\Delta\kappa)\Delta\kappa} \left[\sqrt{(1-\sum_{i+j=n}^{i\geq j\geq 0} b_p^2(\kappa_i,\kappa_j))}\cos\big((n\Delta\kappa)(m\Delta x)-\phi_n\big) + \sum_{i+j=n}^{i\geq j\geq 0}|b_p(\kappa_i,\kappa_j)|\cos\big((n\Delta\kappa)(m\Delta x)-(\phi_i+\phi_j+\beta(\kappa_i,\kappa_j))\big)\right] \tag{54}$$

From Euler's notation we have that $e^{\imath\phi} = \cos\phi + \imath\sin\phi$, hence $\cos\phi = \Re[e^{\imath\phi}]$. Applying Euler's notation, we have

$$A(m\Delta x) = \sqrt{2}\sum_{n=0}^{\infty}\sqrt{2S(n\Delta\kappa)\Delta\kappa} \Re\Big[\sqrt{(1-\sum_{i+j=n}^{i\geq j\geq 0} b_p^2(\kappa_i,\kappa_j))}e^{\imath\left((n\Delta\kappa)(m\Delta x)-\phi_n\right)} + \sum_{i+j=k}^{i\geq j\geq 0}|b_p(\kappa_i,\kappa_j)|e^{\imath\left((n\Delta\kappa)(m\Delta x)-(\phi_i+\phi_j+\beta(\kappa_i,\kappa_j))\right)}\Big] \tag{55}$$

which can be factored as

$$A(m\Delta x) = \sqrt{2}\sum_{n=0}^{\infty}\sqrt{2S(n\Delta\kappa)\Delta\kappa} \Re\Big[\left(e^{\imath\left((n\Delta\kappa)(m\Delta x)\right)}\right)\left(\sqrt{(1-\sum_{i+j=n}^{i\geq j\geq 0} b_p^2(\kappa_i,\kappa_j))}e^{-\imath\phi_n} + \sum_{i+j=n}^{i\geq j\geq 0}|b_p(\kappa_i,\kappa_j)|e^{-\imath(\phi_i+\phi_j+\beta(\kappa_i,\kappa_j))}\right)\Big] \tag{56}$$

The standard form for implementation of the FFT is given by [48]:

$$A_m = \sum_{n=0}^{N-1} B_n e^{-2\pi\imath\frac{mn}{N}} \tag{57}$$

By grouping terms in Eq. (56) as follows,

$$A(m\Delta x) = \Re\Big[\sum_{n=0}^{\infty} B_n e^{i\left((n\Delta\kappa)(m\Delta x)\right)}\Big]$$
$$\text{where } B_n = \sqrt{2}C_n\left[\sqrt{(1-\sum_{i+j=n}^{i\geq j\geq 0} b_p^2(\kappa_i,\kappa_j))}e^{i\phi_n} + \sum_{i+j=n}^{i\geq j\geq 0}|b_p(\kappa_i,\kappa_j)|e^{i(\phi_i+\phi_j+\beta(\kappa_i,\kappa_j))}\right]$$
$$C_n = \sqrt{2S(n\Delta\kappa)\Delta\kappa} \tag{58}$$

we see that the simulation formula in Eq. (56) can be expressed in the compact form of the FFT operator in Eq. (57).

For illustration of the implementation here, we will adopt the following shorthand notation. Let $\boldsymbol{A} = \{A_m; m = 0,\dots M-1\}$ where $A_m = A(m\Delta x)$ and $\boldsymbol{B} = \{B_n; n = 0,\dots,N-1\}$ where $B_n = B(n\Delta\kappa)$, then the fast Fourier transform will be expressed as $\boldsymbol{A} = \text{FFT}(\boldsymbol{B})$. Similarly, the inverse FFT is denoted $\boldsymbol{A} = \text{IFFT}(\boldsymbol{B})$. Practically speaking, the FFT implementation involves typically a $\frac{1}{N}$ normalization term and therefore inverse FFT requires a multiplication by N. With this shorthand, the simulation formula can be expressed as

$$\boldsymbol{A} = \Re\{N\,\text{IFFT}(\boldsymbol{B})\} \tag{59}$$

5.5. Simulation of d-dimensional random fields with FFT

The fully discretized simulation formula for d-dimensional random fields is given as follows:

$$A(m_1\Delta x_1, m_2\Delta x_2,\dots,m_d\Delta x_d) = \sum_{n_d=-N_d}^{N_d}\cdots\sum_{n_2=-N_2}^{N_2}\sum_{n_1=0}^{N_1}\Big[\sqrt{2}\sqrt{2S_p(n_1\Delta\kappa_1, n_2\Delta\kappa_2\dots n_d\Delta\kappa_d)\Delta\kappa_1\Delta\kappa_2\dots\Delta\kappa_d} \cos(n_1m_1\Delta\kappa_1\Delta x_1 + n_2m_2\Delta\kappa_2\Delta x_2\dots n_dm_d\Delta\kappa_d\Delta x_d + \Phi_{n_1n_2\dots n_d}) + \sum_{i_1+j_1=n_1}^{i_1\geq j_1\geq 0}\ \sum_{i_2+j_2=n_2}^{|n_2|\geq|i_2|\geq|j_2|\geq 0}\cdots\sum_{i_d+j_d=n_d}^{|n_d|\geq|i_d|\geq|j_d|\geq 0} \sqrt{2}\sqrt{2S(n_1\Delta\kappa_1, n_2\Delta\kappa_2\dots n_d\Delta\kappa_d)\Delta\kappa_1\Delta\kappa_2\dots\Delta\kappa_d} b_p(i_1\Delta\kappa_1, j_1\Delta\kappa_1, i_2\Delta\kappa_2, j_2\Delta\kappa_2\dots\dots i_d\Delta\kappa_d, j_d\Delta\kappa_d) \cos(n_1m_1\Delta\kappa_1\Delta x_1 + n_2m_2\Delta\kappa_2\Delta x_2\dots n_dm_d\Delta\kappa_d\Delta x_d + \Phi_{i_1i_2\dots i_d} + \Phi_{j_1j_2\dots j_d} + \beta(i_1\Delta\kappa_1, j_1\Delta\kappa_1, i_2\Delta\kappa_2, j_2\Delta\kappa_2,\dots,\dots i_d\Delta\kappa_d, j_d\Delta\kappa_d))\Big] \tag{60}$$

where (see equation given in Box I).

Following similar steps involved in the development of the FFT implementation for 1D-1V random field, the simulation formula for d-dimensional random fields is given in Box II. This can be simplified to a form amenable to the FFT implementation as

$$A(m_1\Delta x_1, m_2\Delta x_2,\dots,m_d\Delta x_d) = 2\sum_{n_d=0}^{N_d}\cdots\sum_{n_2=0}^{N_2}\sum_{n_1=0}^{N_1}\sum_{I_1=1,I_2=\pm1,\dots,I_d=\pm1}\left[B^{I_1I_2\dots I_d}_{n_1n_2\dots n_d}e^{\imath(I_1n_1m_1\Delta\kappa_1\Delta x_1+I_2n_2m_2\Delta\kappa_2\Delta x_2+\cdots+I_dn_dm_d\Delta\kappa_d\Delta x_d)}\right] \tag{63}$$

Again, expressing this in terms of FFT and IFFT operations the following results:

$$\boldsymbol{A} = 2\left[\sum_{I_1=1,I_2=\pm1,\dots,I_d=\pm1}\Re\{N^J\text{FFT}^{I_d}_{\kappa_d}\circ\text{FFT}^{I_{d-1}}_{\kappa_{d-1}}\circ\dots\circ\text{FFT}^{I_1}_{\kappa_1}(\boldsymbol{B}^{I_1I_2\dots I_d})\}\right] \tag{64}$$

where

$$J = \sum_{j=1}^{d}\hat{I}_j,\quad \hat{I}_j = 1 \text{ if } I_j = 1,\qquad \hat{I}_j = 0 \text{ otherwise} \tag{65}$$

FFT^{I_j} equals IFFT if $I_j = 1$ and FFT if $I_j = -1$, and $\boldsymbol{B}^{I_1I_2\dots I_d}$ are the dth-order tensors having components $B^{I_1I_2\dots I_d}_{n_1n_2\dots n_d}$ in Eq. (63). For example, we can express the simulation formula in 2D compactly in terms of FFTs as

$$\boldsymbol{A} = 2\left[\Re\{N^2(\text{IFFT}_{\kappa_2}\circ\text{IFFT}_{\kappa_1}(\boldsymbol{B}^{11})) + N(\text{FFT}_{\kappa_2}\circ\text{IFFT}_{\kappa_1}(\boldsymbol{B}^{1-1}))\}\right] \tag{66}$$

where the subscript κ_1 or κ_2 specifies the axis of the matrix over which the FFT/IFFT operates. Similarly, the 3-dimensional implementation takes the following form:

$$\boldsymbol{A} = \Re\{N^3\text{IFFT}_{\kappa_3}\circ\text{IFFT}_{\kappa_2}\circ\text{IFFT}_{\kappa_1}(\boldsymbol{B}^{111}) + N^2\text{FFT}_{\kappa_3}\circ\text{IFFT}_{\kappa_2}\circ\text{IFFT}_{\kappa_1}(\boldsymbol{B}^{11-1}) + N^2\text{IFFT}_{\kappa_3}\circ\text{FFT}_{\kappa_2}\circ\text{IFFT}_{\kappa_1}(\boldsymbol{B}^{1-11}) + N\text{FFT}_{\kappa_3}\circ\text{FFT}_{\kappa_2}\circ\text{IFFT}_{\kappa_1}(\boldsymbol{B}^{1-1-1})\} \tag{67}$$

In the case of quadrant random fields, the FFT implementation can be further simplified to

$$A(m_1\Delta x_1, m_2\Delta x_2,\dots,m_d\Delta x_d) = 2\sum_{n_d=0}^{N_d}\cdots\sum_{n_2=0}^{N_2}\sum_{n_1=0}^{N_1} B_{n_1n_2\dots n_d}\left[e^{\imath(n_1m_1\Delta\kappa_1\Delta x_1)}(e^{\imath(n_2m_2\Delta\kappa_2\Delta x_2)} + e^{-\imath(n_2m_2\Delta\kappa_2\Delta x_2)})\dots(e^{\imath(n_dm_d\Delta\kappa_d\Delta x_d)} + e^{-\imath(n_dm_d\Delta\kappa_d\Delta x_d)})\right] \tag{68}$$

$$S_p(n_1\Delta\kappa_1, n_2\Delta\kappa_2, \dots, n_d\Delta\kappa_d) = S(n_1\Delta\kappa_1, n_2\Delta\kappa_2, \dots, n_d\Delta\kappa_d) \times \left(1 - \sum_{i_1+j_1=n_1}^{i_1\geq j_1\geq 0} \sum_{i_2+j_2=n_2}^{|n_2|\geq|i_2|\geq|j_2|\geq 0} \cdots \sum_{i_d+j_d=n_d}^{|n_d|\geq|i_d|\geq|j_d|\geq 0} b_p^2(i_1\Delta\kappa_1, j_1\Delta\kappa_1, i_2\Delta\kappa_2, j_2\Delta\kappa_2, \dots, i_d\Delta\kappa_d, j_d\Delta\kappa_d)\right) \tag{61}$$

$$b_p^2(i_1\Delta\kappa_1, j_1\Delta\kappa_1, i_2\Delta\kappa_2, j_2\Delta\kappa_2, \dots, i_d\Delta\kappa_d, j_d\Delta\kappa_d) = \frac{|B(i_1\Delta\kappa_1, j_1\Delta\kappa_1, i_2\Delta\kappa_2, j_2\Delta\kappa_2, \dots, i_d\Delta\kappa_d, j_d\Delta\kappa_d)|^2\Delta\kappa_1\Delta\kappa_2\dots\Delta\kappa_d}{S_p(i_1\Delta\kappa_1, i_2\Delta\kappa_2, \dots, i_d\Delta\kappa_d)S_p(j_1\Delta\kappa_1, j_2\Delta\kappa_2, \dots, j_d\Delta\kappa_d)S((i_1+j_1)\Delta\kappa_1, \dots, (i_d+j_d)\Delta\kappa_d)}$$

Box I.

$$A(m_1\Delta x_1, m_2\Delta x_2, \dots, m_d\Delta x_d) = 2\sum_{n_d=0}^{N_d}\cdots\sum_{n_2=0}^{N_2}\sum_{n_1=0}^{N_1}\sum_{I_1=1, I_2=\pm1, \dots, I_d=\pm1} \sqrt{S(I_1n_1\Delta\kappa_1, I_2n_2\Delta\kappa_2, \dots, I_dn_d\Delta\kappa_d)\Delta\kappa_1\Delta\kappa_2\dots\Delta\kappa_d} \Bigg[\sqrt{(1 - \sum_{i_1+j_1=I_1n_1}^{i_1\geq j_1\geq 0} \sum_{i_2+j_2=I_2n_2}^{n_2\geq|i_2|\geq|j_2|\geq 0} \cdots \sum_{i_d+j_d=I_dn_d}^{n_d\geq|i_d|\geq|j_d|\geq 0} b_p^2(i_1\Delta\kappa_1, j_1\Delta\kappa_1, i_2\Delta\kappa_2, j_2\Delta\kappa_2, \dots, \dots i_d\Delta\kappa_d, j_d\Delta\kappa_d)} e^{\imath\Phi^{I_1I_2\dots I_d}_{n_1n_2\dots n_d}} + \sum_{i_1+j_1=I_1n_1}^{i_1\geq j_1\geq 0} \sum_{i_2+j_2=I_2n_2}^{n_2\geq|i_2|\geq|j_2|\geq 0} \cdots \sum_{i_d+j_d=I_dn_d}^{n_d\geq|i_d|\geq|j_d|\geq 0} b_p(i_1\Delta\kappa_1, j_1\Delta\kappa_1, i_2\Delta\kappa_2, j_2\Delta\kappa_2, \dots, \dots i_d\Delta\kappa_d, j_d\Delta\kappa_d) \times e^{\imath(\Phi^{I_1I_2\dots I_d}_{i_1i_2\dots i_d} + \Phi^{I_1I_2\dots I_d}_{j_1j_2\dots j_d} + \beta(i_1\Delta\kappa_1, j_1\Delta\kappa_1, i_2\Delta\kappa_2, j_2\Delta\kappa_2, \dots, \dots i_d\Delta\kappa_d, j_d\Delta\kappa_d))}\Bigg] e^{\imath(I_1n_1m_1\Delta\kappa_1\Delta x_1 + I_2n_2m_2\Delta\kappa_2\Delta x_2 + \cdots + I_dn_dm_d\Delta\kappa_d\Delta x_d)} \tag{62}$$

Box II.

In terms of FFT and IFFT operators, it takes the following form:

$$\boldsymbol{A} = 2\left[\sum_{I_1=1, I_2=\pm1, \dots, I_d=\pm1} \Re\{N^J \mathrm{FFT}^{I_d}_{\kappa_d} \circ \mathrm{FFT}^{I_{d-1}}_{\kappa_{d-1}} \circ \dots \circ \mathrm{FFT}^{I_1}_{\kappa_1}(\boldsymbol{B})\}\right] \tag{69}$$

where $\boldsymbol{B}$ is the dth-order tensor having terms $B_{n_1n_2\dots n_d}$ in Eq. (68). Detailed development for the simulation of 2D random fields with the use of FFT is provided in [44].

5.6. Notes on the use of the FFT technique

It is well known that the application of the FFT technique requires that certain conditions be satisfied. One such condition relates the spatial and wave number discretizations as follows:

$$\Delta\kappa_1\Delta x_1 = \frac{2\pi}{N_1}, \quad \Delta\kappa_2\Delta x_2 = \frac{2\pi}{N_2}, \quad \dots, \quad \Delta\kappa_d\Delta x_d = \frac{2\pi}{N_d} \tag{70}$$

This is equivalent to a condition that the spatial domain over which the samples are generated is always equal to one period.

The general procedure for simulating d-dimensional third-order random fields with the FFT implementation is as follows:

1. Assign the appropriate wave number discretization over the d dimensions of the power spectrum and the bispectrum. Associated spatial increments follow from Eq. (70).
2. Ensure that the spatial increments satisfy the conditions in Eq. (47) to avoid aliasing.
3. Generate the necessary 2^{d-1}, dth-order random phase tensors $\boldsymbol{\Phi}^{I_1I_2\dots I_d}$ for general fields or a single dth-order random phase tensor for quadrant random fields.
4. Compute the 2^{d-1}, dth-order spectral tensors $\boldsymbol{B}^{I_1I_2\dots I_d}$ for general fields or a single dth-order spectral tensor for quadrant random fields.
5. Apply FFT and IFFT appropriately along the different axes of the d-dimensional spectral tensor(s) $\boldsymbol{B}$ according to the equations above.

The major advantage of the FFT implementation is computational expense. Each FFT has well-known complexity of the order $O(M\log N)$, whereas each summation of cosines has complexity of the order $O(MN)$. Because the summations in the original formulation are nested over each dimension, the complexity grows exponentially with dimension as $O((MN)^d)$. However, as we can see from the above expressions, the FFT implementation requires only $2^{d-1}d$ FFTs and therefore has complexity of order $O(d2^{d-1}M\log N) \ll O((MN)^d)$. For quadrant random fields, this is reduced even further having order $O(2dM\log N)$ and therefore only scales linearly with dimension.

The result is a drastic reduction in the computational time, without which the simulation of multidimensional higher-order random fields becomes infeasible. To illustrate the savings, Table 1 shows a comparison of the computation time for the non-FFT and the FFT implementations for a 1-dimensional random field for different number of sample functions generated. On average the FFT calculations are three orders of magnitude faster.

While Table 1 illustrates the huge savings for one-dimensional fields, it is particularly interesting to observe how these computation times scale with dimension. Table 2 shows that computation times for 2- and 3-dimensional random fields using the FFT implementation remain modest. Note, however, that we do not compare with the summation of cosines here because these calculations become intractable for dimensions greater than one. All the simulations are performed on a MacBook Pro 2017 using 3.1 GHz Dual-Core Intel Core i5 CPU and 8 GB 2133 MHz LPDDR3 memory.

6. Simulation of ergodic multi-variate stochastic processes by 3rd-order spectral representation method

Thus far, we have established the equations for the simulation of 1D-1V random process and nD-1V random fields. To simulate the 1D-mV stationary stochastic vector process $[f_1(t), f_2(t), \dots \dots f_m(t)]^T$, the pure component of the 2nd-order cross spectral density $S_p(\omega)$ must be computed first. In case of a simple 1D-1V stationary stochastic processes, the computation is straightforward, see Eq. (14). However,

Table 1
Comparison of the computation time for simulation of 1D third-order random fields using the standard and FFT implementations.

No. of samples	Time (s)	
	Standard	FFT
128	14.842	0.0893
512	26.891	0.0957
1024	48.383	0.1399
2048	82.525	0.3750
4096	456.100	1.9270

Table 2
Computational time for the simulation of 2D and 3D third-order random fields using the FFT implementation. Standard implementation is not shown because the calculations are impractical on a desktop computer.

No. of samples	Time (s)	
	2D	3D
1	0.224	20.651
16	0.225	21.839
128	0.274	25.600
512	0.375	37.89

the pure cross-spectral density for a stochastic vector process is not trivial, and requires us to resort to Einstein (tensor) notation. The pure cross-spectral density is thus expressed as

$$S^{p}_{ab}(\omega_k) = S_{ab}(\omega_k) - \sum_{i+j=k}^{i\geq j>0} B_{aef}(\omega_i,\omega_j)B^{*}_{bgh}(\omega_i,\omega_j)G_{pe}(\omega_i) \times G_{pg}(\omega_i)G_{qf}(\omega_j)G_{qh}(\omega_j)\Delta\omega^2 \tag{71}$$

where the term $G(\omega)$ is the inverse of the decomposed pure cross-spectral density derived as follows. Similar to the 2nd-order expansion, the pure cross-spectral density can be decomposed using the eigenvalue decomposition as

$$S^{(p)}(\omega) = H(\omega)H^{T*}(\omega) \tag{72}$$

and having the following properties

$$H_{jj}(\omega) = H_{jj}(-\omega), H_{jk}(\omega) = H^{*}_{jk}(-\omega), H_{jk}(\omega) = |H_{jk}(\omega)|e^{\imath\theta_{jk}(\omega)}, \quad \theta_{jk}(\omega) = \tan^{-1}\left(\frac{\Im[H_{jk}(\omega)]}{\Re[H_{jk}(\omega)]}\right) \tag{73}$$

We then define $G(\omega) = (H(\omega))^{-1}$, which again can be expressed in polar coordinates as:

$$G_{jk}(\omega) = |G_{jk}(\omega)|e^{\imath\theta^{I}_{jk}(\omega)}, \theta^{I}_{jk}(\omega) = \tan^{-1}\left(\frac{\Im[G_{jk}(\omega)]}{\Re[G_{jk}(\omega)]}\right) \tag{74}$$

Leveraging these quantities, the stochastic vector process $f_a(t); a = 1, 2, \ldots m$ can be simulated as follows:

$$f_a(t) = 2\sum_{k=0}^{N-1}\Big[\sum_{l=1}^{m}|H_{al}(\omega_{lk})|\sqrt{\Delta\omega}\cos(\omega_{lk}t - \theta_{al}(\omega_{lk}) + \phi_{lk}) + 2\sum_{l=1}^{m}\sum_{n=1}^{m}\sum_{p=1}^{m}\sum_{q=1}^{m}\sum_{i+j=k}^{i\geq j\geq 0}|B_{aln}(\omega_{pi},\omega_{qj})||G_{lp}(\omega_{pi})||G_{nq}(\omega_{qj})|\Delta\omega \cos((\omega_{pi}+\omega_{qj})t - \beta_{aln}(\omega_{pi},\omega_{qj}) - \theta^{I}_{lp}(\omega_{pi}) - \theta^{I}_{nq}(\omega_{qj}) + \phi_{pi} + \phi_{qj})\Big] \tag{75}$$

where

$$\beta_{aln}(\omega_{pi},\omega_{qj}) = \tan^{-1}\left(\frac{\Im[B_{aln}(\omega_{pi},\omega_{qj})]}{\Re[B_{aln}(\omega_{pi},\omega_{qj})]}\right) \tag{76}$$

is the biphase, and

$$\omega_{lk} = k\Delta\omega + \frac{l}{2m}\Delta\omega + \frac{1}{N}\Delta\omega \tag{77}$$

The stochastic vector processes simulated using Eq. (75) satisfy both ensemble and ergodic properties of the vector process up to the third order. Further details along with proofs can be found in [49].

6.1. Simulation of stochastic vector processes by FFT

The simulation formula for stochastic vector processes presented above in Eq. (75) is computationally expensive, but can be accelerated with the FFT. Again, applying Euler's formula, $e^{\imath\phi} = \cos(\phi) + \imath\sin(\phi)$, such that $\Re[e^{\imath\phi}] = \cos(\phi)$, the simulation formula simplifies to

$$f_a(t) = \Re\Big[2\sum_{k=0}^{N-1}\Big[\sum_{l=1}^{m}|H_{al}(\omega_{lk})|\sqrt{\Delta\omega}e^{\imath(\omega_{lk}t-\theta_{al}(\omega_{lk})+\phi_{lk})} + \sum_{l=1}^{m}\sum_{n=1}^{m}\sum_{p=1}^{m}\sum_{q=1}^{m}\sum_{i+j=k}^{i\geq j\geq 0}|B_{aln}(\omega_{pi},\omega_{qj})||G_{lp}(\omega_{pi})||G_{nq}(\omega_{qj})|\Delta\omega e^{\imath(\omega_{pi}+\omega_{qj})t-\beta_{aln}(\omega_{pi},\omega_{qj})-\theta^{I}_{lp}(\omega_{pi})-\theta^{I}_{nq}(\omega_{qj})+\phi_{pi}+\phi_{qj}}\Big]\Big] \tag{78}$$

Discretizing the time domain using $t_r = r\Delta t$ and the frequency domain using the multi-indexed frequency in Eq. (77) yields

$$f_a(r\Delta t) = \Re\Big[2\sum_{k=0}^{N-1}\Big[\sum_{l=1}^{m}|H_{al}(\omega_{lk})|\sqrt{\Delta\omega}e^{\imath(\frac{lr}{2m}+\frac{1}{N})\Delta\omega\Delta t}e^{\imath(-\theta_{al}(\omega_{lk})+\phi_{lk})} + \sum_{l=1}^{m}\sum_{n=1}^{m}\sum_{p=1}^{m}\sum_{q=1}^{m}\sum_{i+j=k}^{i\geq j\geq 0}|B_{aln}(\omega_i,\omega_j)||G_{lp}(\omega_i)||G_{nq}(\omega_j)|\Delta\omega e^{\imath(\frac{pr}{2m}+\frac{qr}{2m}+\frac{2}{N})\Delta\omega\Delta t}e^{\imath(-\beta_{aln}(\omega_{pi},\omega_{qj})-\theta^{I}_{lp}(\omega_{pi})-\theta^{I}_{nq}(\omega_{qj})+\phi_{pi}+\phi_{qj})}\Big]e^{\imath kr\Delta\omega\Delta t}\Big] \tag{79}$$

Expressing this equation in terms of the standard FFT implementation, we have

$$f_a(r\Delta t) = \Re\Big[\sum_{k=0}^{N-1}C_k e^{\imath kr\Delta\omega\Delta t}\Big] \tag{80}$$

where C_k is given by

$$C_k = 2\Big[\sum_{l=1}^{m}|H_{al}(\omega_{lk})|\sqrt{\Delta\omega}e^{\imath(-\theta_{al}(\omega_{lk})+\phi_{lk})} + \sum_{i+j=k}^{i\geq j\geq 0}\sum_{l=1}^{m}\sum_{n=1}^{m}\sum_{p=1}^{m}\sum_{q=1}^{m}|B_{aln}(\omega_{pi},\omega_{qj})||G_{lp}(\omega_{pi})||G_{nq}(\omega_{qj})| \times \Delta\omega e^{\imath(-\beta_{aln}(\omega_{pi},\omega_{qj})-\theta^{I}_{lp}(\omega_{pi})-\theta^{I}_{nq}(\omega_{qj})+\phi_{pi}+\phi_{qj})}\Big] \tag{81}$$

and we have the following conditions to ensure the ergodicity and avoid aliasing

$$m\Delta t = T_0 = m\frac{2\pi}{\Delta\omega}, \quad \Delta t = \frac{2\pi}{m\Delta\omega} \tag{82}$$

Simulation by FFT using Eq. (80) and (81) saves considerable computational expense while retaining the desired ensemble and ergodicity properties of the sample functions.

7. Numerical examples

In this section, we present examples of the simulation of skewed 2- and 3-dimensional random fields from prescribed power spectra and bispectra. These examples, although purely mathematical in nature and not corresponding to any physically meaningful random field, have been developed to call attention to specific features of the proposed methodology. Finally, we also present an example of the simulation of a stochastic vector process.

7.1. Comparison of 2-dimensional 2nd- and 3rd-order random fields

The first example compares the simulation of a 2-dimensional random field by the 2nd-order SRM and the 3rd-order SRM. The prescribed

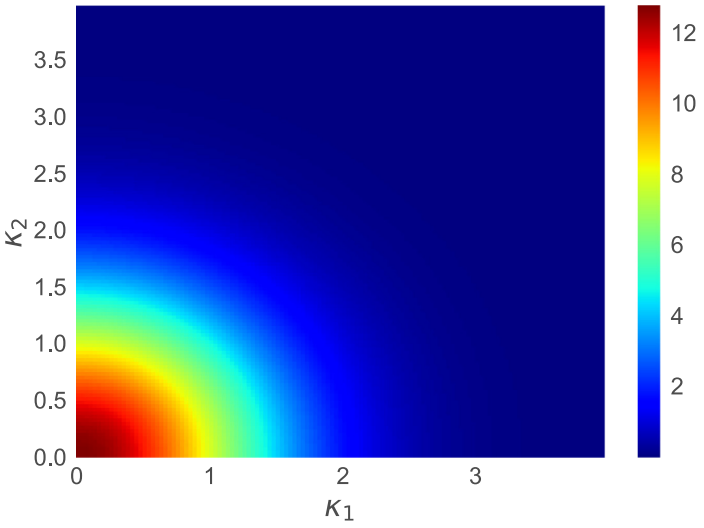

Fig. 1. 2-dimensional power spectrum.

power spectrum is given by

$$S(\kappa_1,\kappa_2) = \frac{40}{\pi}\exp-\frac{1}{2}(\kappa_1^2+\kappa_2^2) \text{ for } \kappa_1,\kappa_2 \geq 0 \tag{83}$$

and is plotted in Fig. 1, yielding a random field with zero mean and variance 75. Notice that the power spectrum is radially symmetric. The prescribed bispectrum for the 3rd-order random field is given by

$$\begin{aligned}\Re B(\kappa_{11},\kappa_{12},\kappa_{21},\kappa_{22}) &= \Im B(\kappa_{11},\kappa_{12},\kappa_{21},\kappa_{22})\\ &= \frac{210}{\pi^2}\exp-(\kappa_{11}^2+\kappa_{12}^2+\kappa_{21}^2+\kappa_{22}^2)\\ &\text{for } \kappa_{11},\kappa_{12},\kappa_{21},\kappa_{22}\geq 0\end{aligned} \tag{84}$$

Visualization of the 2-dimensional bispectrum, which is a 4th-order tensor, is not trivial. Of particular note is that the bispectrum is symmetric across all dimensions, i.e. it has the same rate of decay along each axis. This implies that the coupling of the waves is the same in both dimensions.

One thousand samples of the 2nd- and 3rd-order random fields are simulated using the SRM with the following parameters.

$$\begin{aligned}&\Delta x_1 = \Delta x_2 = 0.7853, \quad \Delta\kappa_1 = \Delta\kappa_2 = 0.03125,\\ &N_1 = N_2 = 128, \quad M_1 = M_2 = 256\end{aligned} \tag{85}$$

The cutoff frequency is $\kappa_u = 4$ rad/sec and the value of ϵ from Eqs. (37)–(38) is determined as

$$\begin{aligned}&\int_0^4\int_{-4}^4 S(\kappa_1,\kappa_2)d\kappa_1 d\kappa_2 = (1-\epsilon)\int_0^\infty\int_{-\infty}^\infty S(\kappa_1,\kappa_2)d\kappa_1 d\kappa_2\\ &2\int_0^4\int_0^4 S(\kappa_1,\kappa_2)d\kappa_1 d\kappa_2 = 2(1-\epsilon)\int_0^\infty\int_0^\infty S(\kappa_1,\kappa_2)d\kappa_1 d\kappa_2\\ &\epsilon = 0.00012668\end{aligned} \tag{86}$$

Plots of representative 2nd- and 3rd-order sample realizations having identical phase angles are presented in Fig. 2. On initial inspection, both sample realizations look similar. However a closer inspection of the samples and their statistical properties reveals interesting characteristics. The difference between the sample realizations of the 2nd- and 3rd-order random fields is shown in Fig. 2(c). The plot clearly shows that there are significant differences between the two sample realizations. These differences arise from asymmetry introduced by the proposed methodology. Also note that the differences are oriented along a $\arctan(1) = 45°$ and $\arctan(-1) = -45°$ angle relative to the x_1 and x_2 axes. This arises because the form of the bispectrum is identical in both the x_1 and x_2 directions. Consequently, the length-scale associated with third-order correlations in the x_1 and x_2 axes are the same — resulting in the 45° and −45° "bands" of skewness.

Table 3
Example 1: Target and estimated moments of random fields generated by the 2nd and 3rd-order SRM.

Moments	Target	3rd-order	2nd-order
Mean	0.00	−0.001	−0.001
Variance	80	81.99	81.98
Skewness	0.22	0.2079	0.0004

Statistical properties, estimated from the 1000 sample realizations, are presented in Table 3, illustrating the ability of the proposed methodology to match the theoretical properties up to third-order. The original SRM, on the other hand, matches the properties of the process only up to second-order. Fig. 3 further shows the convergence of variance and skewness of the 2D samples generated with increasing number of samples. We see that there is some small discrepancy between the theoretical and simulated statistics, even after 1000 samples. Much of this discrepancy can be attributed to the frequency discretization. Fig. 3 shows the convergence of variance and skewness with increasing number of frequency intervals with constant cutoff frequency $\kappa_{1u} = \kappa_{2u} = 4$ rad/sec, which maintains a theoretical accuracy given in Eq. (86).

7.2. 2-dimensional random fields with different bispectra

In the second example, we modify the bispectrum such that wave interactions occur on different length-scales in the κ_1 and κ_2 directions and illustrate how the asymmetric features of random field differ with these relative length-scales. We generate two sets of random fields with the same power spectrum given above in Eq. (83) and shown in Fig. 1. However, we consider two different bispectra as follows

$$\begin{aligned}\Re B_1(\kappa_{11},\kappa_{12},\kappa_{21},\kappa_{22}) &= \Im B_1(\kappa_{11},\kappa_{12},\kappa_{21},\kappa_{22})\\ &= \frac{500}{\pi^2}\exp-(10\kappa_{11}^2+\kappa_{12}^2+10\kappa_{21}^2+\kappa_{22}^2)\end{aligned} \tag{87}$$

$$\begin{aligned}\Re B_2(\kappa_{11},\kappa_{12},\kappa_{21},\kappa_{22}) &= \Im B_2(\kappa_{11},\kappa_{12},\kappa_{21},\kappa_{22})\\ &= \frac{500}{\pi^2}\exp-(\kappa_{11}^2+10\kappa_{12}^2+\kappa_{21}^2+10\kappa_{22}^2)\end{aligned} \tag{88}$$

Again, visualization of the 2-dimensional bispectra is not included.

The first bispectrum shows accelerated decay along the x_1 axis whereas the second bispectrum has accelerated decay along the x_2 axis. Samples are again simulated using the FFT implementation of the 3rd-order SRM. Plots of two sample realizations having the same discretization and random phase angles as Example 1 for direct comparison with the 2nd-order, are presented in Fig. 5.

Again, to the naked eye, the 3rd-order sample realizations look similar to the second-order. But taking the difference between the sample realizations of 2nd- and 3rd-order fields (Fig. 6), we now see that the asymmetric features are elongated along particular axes. In the case of B_1, the asymmetric features lie most prominently along the x_1 axis where the decay in bispectrum is more rapid. Interestingly, the asymmetric features occur at an angle approximately $\arctan(\sqrt{10}) \approx 73°$ and $\arctan(-\sqrt{10}) \approx -73°$ from the x_2 axis (or $\arctan(\sqrt{0.1}) \approx 18°$ and $\arctan(-\sqrt{0.1}) \approx -18°$ from the x_1 axis) indicative of a 10:1 aspect ratio of the nonlinear features. The inverse is true for B_2.

Lastly, we generated 1000 samples of the 2nd- and 3rd-order random fields and the statistical properties of the sample realizations are presented in Table 4. Again, all of the random fields possess approximately the correct mean and variance. However, only the 3rd-order SRM samples possess the correct skewness. Moreover, they possess the full bispectra but this cannot be visualized.

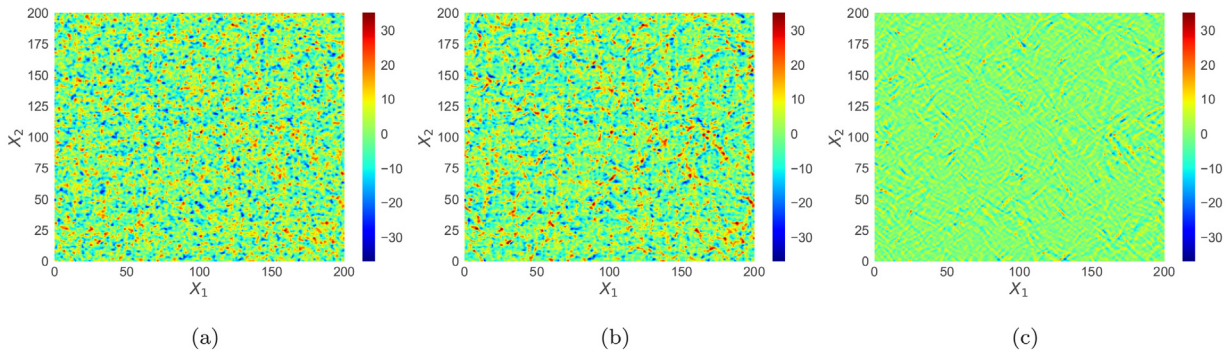

Fig. 2. 3-dimensional random fields simulated by the (a) 2nd-order SRM, (b) 3rd-order SRM and (c) Difference between the 2nd and 3rd SRM.

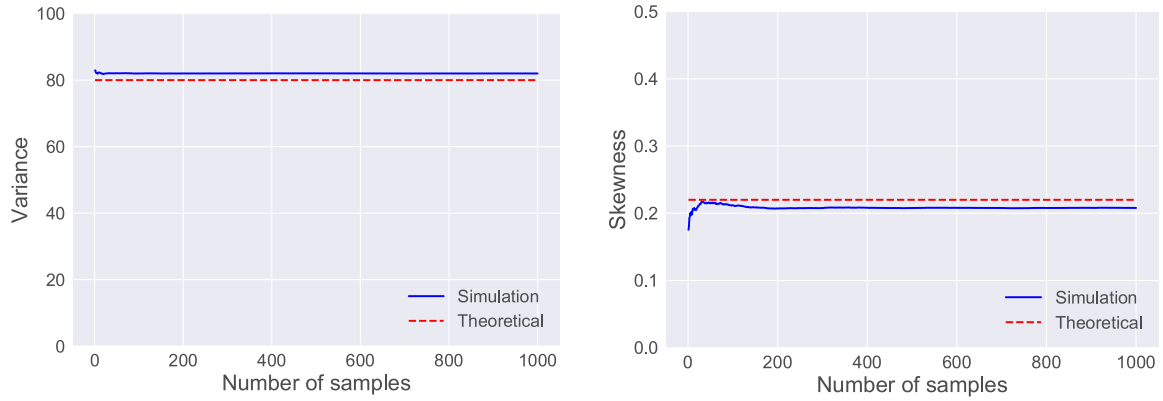

Fig. 3. Convergence of variance and skewness with increasing number of samples.

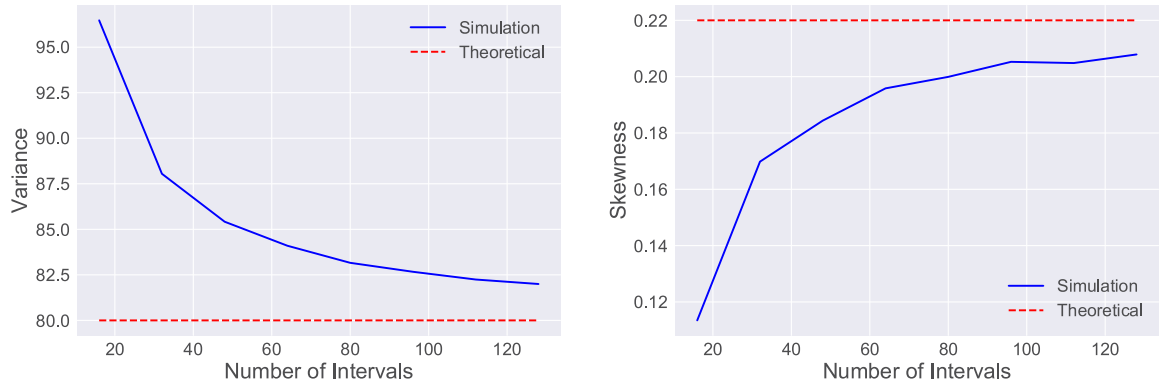

Fig. 4. Convergence of variance and skewness with increasing number of wavenumber intervals.

Table 4
Target and estimated moments of random fields generated by the 2nd and 3rd order SRM.

Moments	Target	3rd-order, B_1	3rd-order, B_2	2nd-order
Mean	0.00	0.0044	0.0044	0.0044
Variance	80	81.990	81.975	81.996
Skewness	0.052	0.04897	0.04846	0.0005

7.3. Comparison of 3-dimensional 2nd- and 3rd-order random fields

In this example, we compare simulations of 3-dimensional random fields having a prescribed power spectrum (2nd-order) and power spectrum and bispectrum (3rd-order). Both random fields have a power spectrum given by:

$$S(\kappa_1,\kappa_2,\kappa_3) = \frac{20}{\sqrt{2\pi}}\exp -\frac{1}{2}(\kappa_1^2+\kappa_2^2+\kappa_3^2) \tag{89}$$

and plotted in Fig. 7. The third-order random field has bispectrum given by

$$\begin{aligned}&\Re B(\kappa_{11},\kappa_{12},\kappa_{21},\kappa_{22},\kappa_{31},\kappa_{32}) = \Im B(\kappa_{11},\kappa_{12},\kappa_{21},\kappa_{22},\kappa_{31},\kappa_{32})\\ &= \frac{22}{2\pi}\exp -(\kappa_{11}^2+\kappa_{12}^2+\kappa_{21}^2+\kappa_{22}^2+\kappa_{31}^2+\kappa_{32}^2)\end{aligned} \tag{90}$$

Visualization of this 3-dimensional bispectrum, which is a 6th-order tensor is not trivial and is therefore not presented here.

One thousand samples with the following discretization were simulated

$$\begin{aligned}&\Delta x_1 = \Delta x_2 = \Delta x_3 = 0.625, \quad \Delta\kappa_1 = \Delta\kappa_2 = \Delta\kappa_2 = 0.314\\ &N_1 = N_2 = N_3 = 16, \quad M_1 = M_2 = M_3 = 32\end{aligned} \tag{91}$$

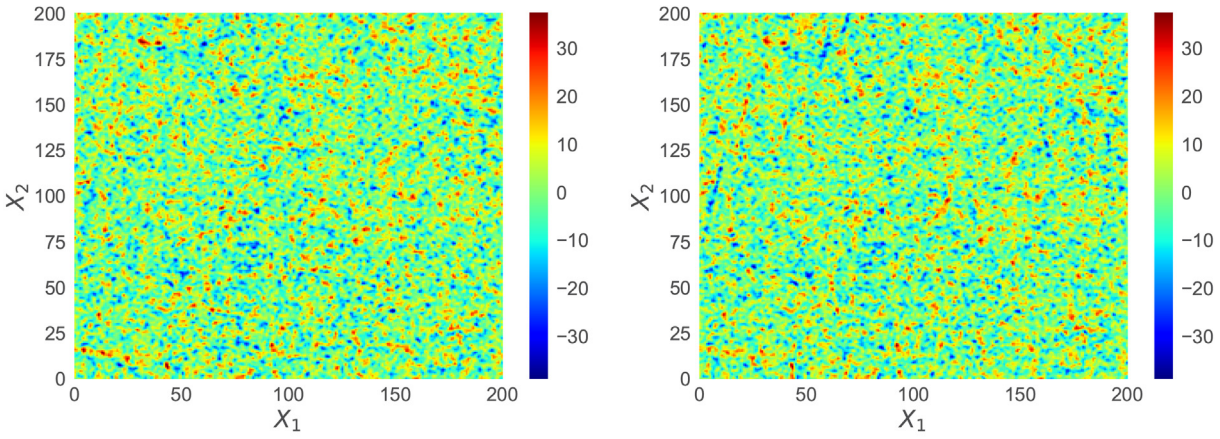

(a) Random field with bispectrum B_1. (b) Random field with bispectrum B_2.

Fig. 5. 2-dimensional random fields generated from the two bispectra using the 3rd-order SRM.

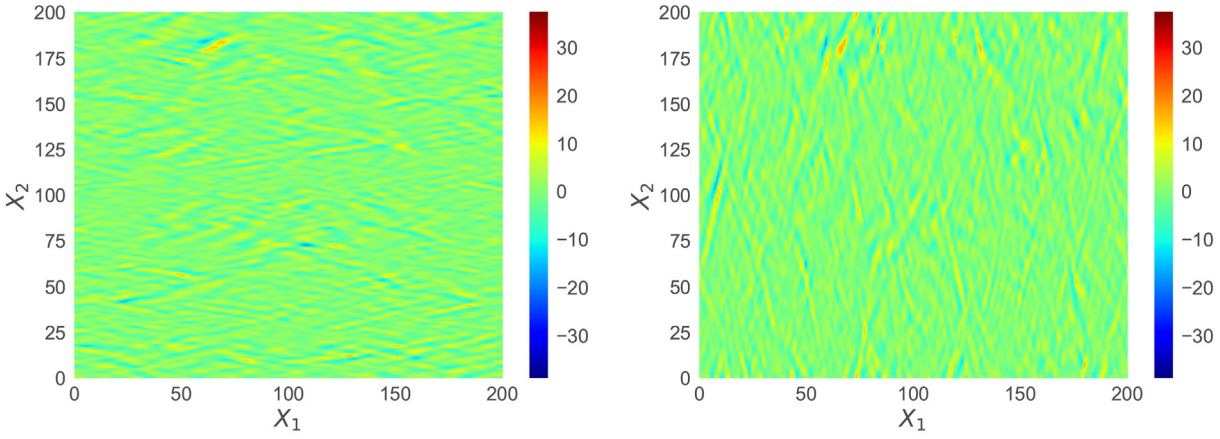

(a) Random field with bispectrum B_1. (b) Random field with bispectrum B_2.

Fig. 6. Difference between samples generated by BSRM and SRM simulations for both the bispectra.

Table 5
Target and estimated moments of random fields generated by the 2nd and 3rd order SRM.

Moments	Target	3rd-order	2nd-order
Mean	0.00	0.0364	0.0364
Variance	179.0812	178.9807	178.9271
Skewness	0.02107	0.02205	0.00081

Plots of representative sample realizations of the 2nd- and 3rd-order random fields, having identical phase angles, are presented in Fig. 8. As in the 2-dimensional case, the sample realizations look similar. The difference between the 2nd- and 3rd-order sample realizations is shown in Fig. 8(c). This difference is the result of the asymmetric non-Gaussianity introduced by the bispectrum. Here, similar to example 1, the asymmetric features in the difference plot are inclined along a 45° and −45° angle along on each plane ($x_1 - x_2$, $x_1 - x_3$, and $x_2 - x_3$) of the sample realization. The similarity of the bispectra across all dimensions gives rise to this.

Sample statistics are given in Table 5 from the 1000 simulations, which demonstrates the ability of the 3rd-order simulations to match the moments up to the skewness. The samples also possess the prescribed bispectrum, but it is not feasible to illustrate this.

7.4. 3-dimensional random fields with different bispectra

Next, we investigate the effects of variations in the bispectrum in 3-dimensional random fields. The random fields simulated here possess the power spectrum from Eq. 7 and illustrated in Fig. 7. We then generate 3rd-order random fields with 3 different bispectra given by

$$\begin{aligned}\Re B_1(\kappa_{11},\kappa_{12},\kappa_{13},\kappa_{21},\kappa_{22},\kappa_{23}) &= \Im B_1(\kappa_{11},\kappa_{12},\kappa_{13},\kappa_{21},\kappa_{22},\kappa_{23}) \\ &= \frac{300}{2\pi}\exp-(10\kappa_{11}^2+\kappa_{12}^2+\kappa_{13}^2+10\kappa_{21}^2+\kappa_{22}^2+\kappa_{23}^2)\end{aligned} \tag{92}$$

$$\begin{aligned}\Re B_2(\kappa_{11},\kappa_{12},\kappa_{13},\kappa_{21},\kappa_{22},\kappa_{23}) &= \Im B_2(\kappa_{11},\kappa_{12},\kappa_{13},\kappa_{21},\kappa_{22},\kappa_{23}) \\ &= \frac{300}{2\pi}\exp-(\kappa_{11}^2+10\kappa_{12}^2+\kappa_{13}^2+\kappa_{21}^2+10\kappa_{22}^2+\kappa_{23}^2)\end{aligned} \tag{93}$$

$$\begin{aligned}\Re B_3(\kappa_{11},\kappa_{12},\kappa_{13},\kappa_{21},\kappa_{22},\kappa_{23}) &= \Im B_3(\kappa_{11},\kappa_{12},\kappa_{13},\kappa_{21},\kappa_{22},\kappa_{23}) \\ &= \frac{300}{2\pi}\exp-(\kappa_{11}^2+\kappa_{12}^2+10\kappa_{13}^2+\kappa_{21}^2+\kappa_{22}^2+10\kappa_{23}^2)\end{aligned} \tag{94}$$

each having the bispectrum decay at a higher rate along a specific axis. For example, the bispectrum B_1 decays more rapidly along the x_1 axis (κ_{11} and κ_{21}).

Plots of the sample realizations from the 3rd-order SRM, having identical phase angles as those in the previous example, are presented

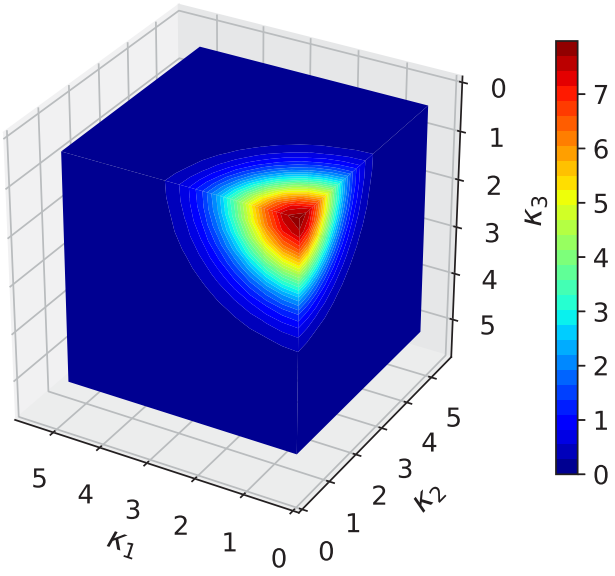

Fig. 7. 3-dimensional power spectrum.

in Fig. 9. As in previous examples, the random field realizations look very similar. Fig. 10 shows the difference between these samples and the 2nd-order field simulated in Fig. 8(a). Here we see that by taking the difference between the samples generated by the 2nd- and 3rd-order Spectral Representation Methods, we have asymmetric features

Table 6
Target and estimated moments of random fields generated by the 2nd and 3rd order SRM.

Moments	Target	3rd-order, B_1	3rd-order, B_2	3rd-order, B_3	2nd-order
Mean	0.00	0.0364	0.0364	0.0364	0.0364
Variance	179.0812	178.9703	178.9787	178.9605	178.9270
Skewness	0.00580	0.00680	0.00682	0.00661	0.0008

elongated along different axes. Specifically, for realizations with bispectrum B_1 have features that are elongated along the x_1-axis, thus the asymmetric features lie along angles of $\arctan(\sqrt{10}) \approx 73°$ and $\arctan(-\sqrt{10}) \approx -73°$ in the $x_1 - x_3$ and $x_1 - x_2$ planes and the features are diagonal (45°) in the $x_2 - x_3$ plane. Likewise, features from B_2 are elongated in x_1 and B_3 are elongated in x_3.

Lastly, 1000 samples with discretization given in Eq. (91) were simulated and the statistics of the resulting random fields were calculated as shown in Table 6. Again, the third-order samples are shown to possess the appropriate 2nd- and 3rd-order statistics. They also possess the proper bispectra, this cannot be feasibly illustrated.

7.5. Comparison of 2nd and 3rd-order stochastic vector process

In the final example, we present the simulation of a tri-variate stochastic vector process representing wind turbulent velocity fluctuations. This example is modified from [30]. Consider three components of the simulated vector process denoted by $f_1(t), f_2(t), f_3(t)$, describing the wind velocity fluctuations at three vertical points in a wind profile (points 1,2 and 3 in Fig. 11).

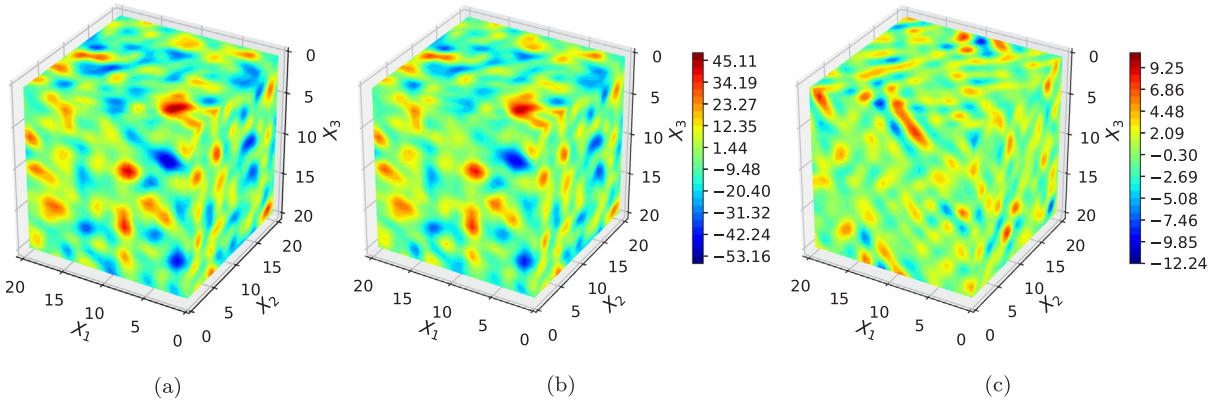

Fig. 8. 3-dimensional random fields simulated by the (a) 2nd-order SRM, (b) 3rd-order SRM and (c) Difference between the 2nd and 3rd SRM.

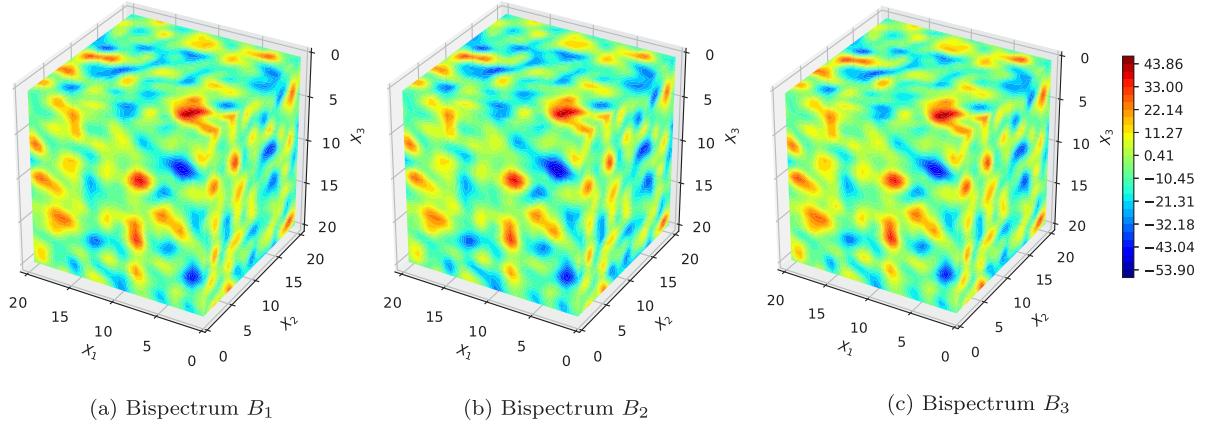

Fig. 9. 3-dimensional random fields generated using 3 different bispectra.

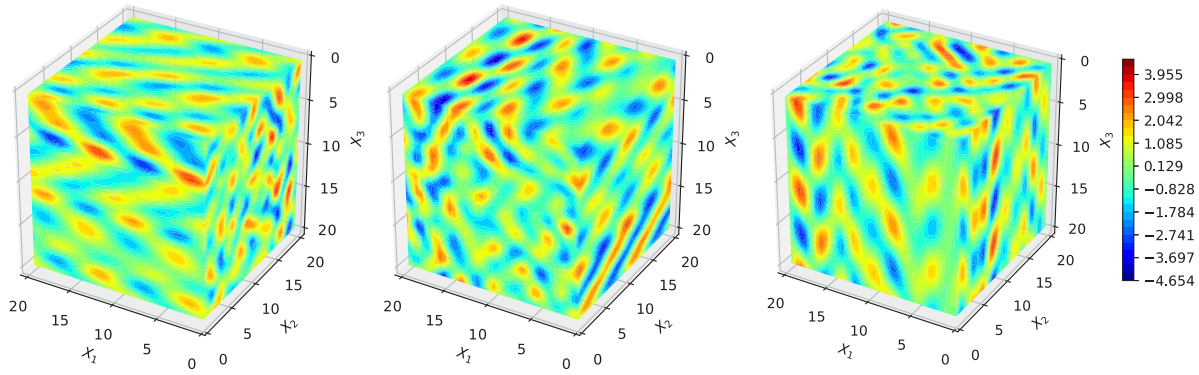

(a) Bispectrum B_1 (b) Bispectrum B_2 (c) Bispectrum B_3

Fig. 10. Difference between 3-dimensional random fields generated using the 2nd- and 3rd-order spectral representation methods.

The components of the 2nd-order cross power spectrum are given by

$$\begin{aligned} S_{jj}(\omega) &= S_j(\omega)\ j = 1,2,3 \\ S_{jk}(\omega) &= \sqrt{S_j(\omega)S_k(\omega)}\gamma_{jk}(\omega)\ j,k = 1,2,3\ j \neq k \end{aligned} \tag{95}$$

where $S_j(\omega)$ is the power spectrum of process $f_j(t)$ and $\gamma_{jk}(\omega)$ is the coherence function between processes $f_j(t)$ and $f_k(t)$. The form suggested by Kaimal [50] is selected to model the 2nd-order cross spectrum of the wind fluctuations and is given by

$$S(z,\omega) = \frac{1}{2}\frac{200}{2\pi}u_*^2\frac{z}{U(z)}\frac{1}{[1+50\frac{\omega z}{2\pi U(z)}]^{\frac{5}{2}}} \tag{96}$$

where z = height above the ground (in m); u_* = shear velocity of the flow (in m/s); and $U(z)$ = mean wind speed at the height z (in m/s). The model suggested in Davenport [51] is selected for the coherence function between the wind velocity fluctuations at different heights given by:

$$\gamma(\Delta z,\omega) = \exp\left[\frac{-\omega}{2\pi}\frac{C_z\Delta z}{\frac{1}{2}[U(z_1)+U(z_2)]}\right] \tag{97}$$

where $U(z_1)$ and $U(z_2)$ are the mean wind speeds at heights z_1 and z_2 respectively, $\Delta z = |z_1 - z_2|$, and C_z is a constant equal to 10. The specific parameter values are obtained from [30] yielding a cross power spectral density given by

$$S_{11} = \frac{38.3}{(1+6.19\omega)^{\frac{5}{3}}},\quad S_{22} = \frac{43.3}{(1+6.98\omega)^{\frac{5}{3}}},\quad S_{33} = \frac{135}{(1+21.8\omega)^{\frac{5}{3}}} \tag{98}$$

and the corresponding coherence functions given by

$$\gamma_{12}(\omega) = e^{-0.1757\omega},\quad \gamma_{13}(\omega) = e^{-3.478\omega},\quad \gamma_{23}(\omega) = e^{-3.292\omega} \tag{99}$$

The spectra and coherences are shown in Fig. 12.

The diagonal components of the 3rd-order cross-spectrum (cross-bispectrum) are assumed to take the following form:

$$\begin{aligned} B_{111}(w_1,w_2) &= \frac{50}{(1+6.19*(w_1+w_2))^{\frac{5}{3}}} \\ B_{222}(w_1,w_2) &= \frac{50}{(1+6.98*(w_1+w_2))^{\frac{5}{3}}} \\ B_{333}(w_1,w_2) &= \frac{50}{(1+21.8*(w_1+w_2))^{\frac{5}{3}}} \end{aligned} \tag{100}$$

while the off-diagonal terms are given by

$$B_{ijk}(w_1,w_2) = \sqrt[3]{B_{iii}(w_1,w_2)B_{jjj}(w_1,w_2)B_{kkk}(w_1,w_2)}\gamma_{ijk} \tag{101}$$

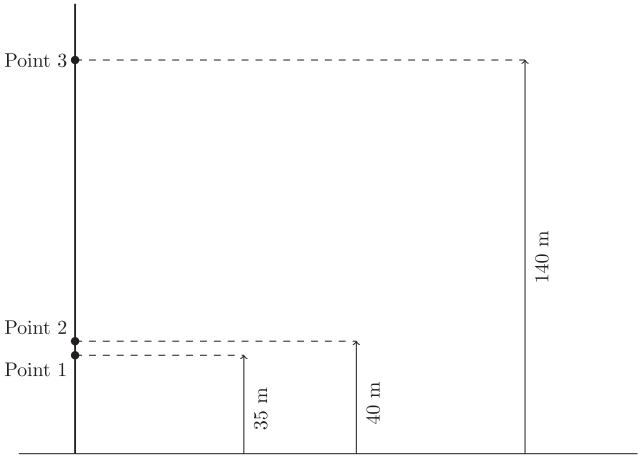

Fig. 11. Configuration of the wind velocity points along a vertical wind profile.

where γ_{ijk} are the third-order coherence functions (or bi-coherences) given by

$$\begin{aligned} &\gamma_{112}(w_1,w_2) = e^{-0.171(w_1+w_2)}, \gamma_{122}(w_1,w_2) = e^{-0.357(w_1+w_2)}, \\ &\gamma_{113}(w_1,w_2) = e^{-1.287(w_1+w_2)}, \gamma_{133}(w_1,w_2) = e^{-1.589(w_1+w_2)}, \\ &\gamma_{123}(w_1,w_2) = e^{-3.473(w_1+w_2)}, \gamma_{223}(w_1,w_2) = e^{-2.659(w_1+w_2)} \\ &\gamma_{233}(w_1,w_2) = e^{-2.775(w_1+w_2)} \end{aligned} \tag{102}$$

Sample functions of this tri-variate stochastic wind velocity process are simulated using Eqs. (80) and (81) with the FFT technique. The upper cutoff frequency and the number of frequency discretizations are given by

$$\omega_u = 2\ \text{rad}/s;\ N_\omega = 100 \tag{103}$$

which results in the following frequency and time discretizations:

$$\Delta\omega = 0.02\ \text{rad}/s;\ \Delta t = 1.57\ sec;\ T_0 = 314.15\ sec \tag{104}$$

A single realization of each vector component is plotted in Fig. 13, which also shows comparisons with sample functions generated using the 2nd-order SRM (having the same random phase angles). To verify that the simulations do, indeed, possess the prescribed statistical properties, the 1st, 2nd and 3rd-order ensemble properties from 1000 simulation are summarized in Tables 7–9. Note that we do not produce plots of the spectral quantities because these are difficult to visualize. From these tables, we see that the first and second-order ensemble moments are very close to the target for both the second and third-order simulations. However, the second-order simulations cannot match the

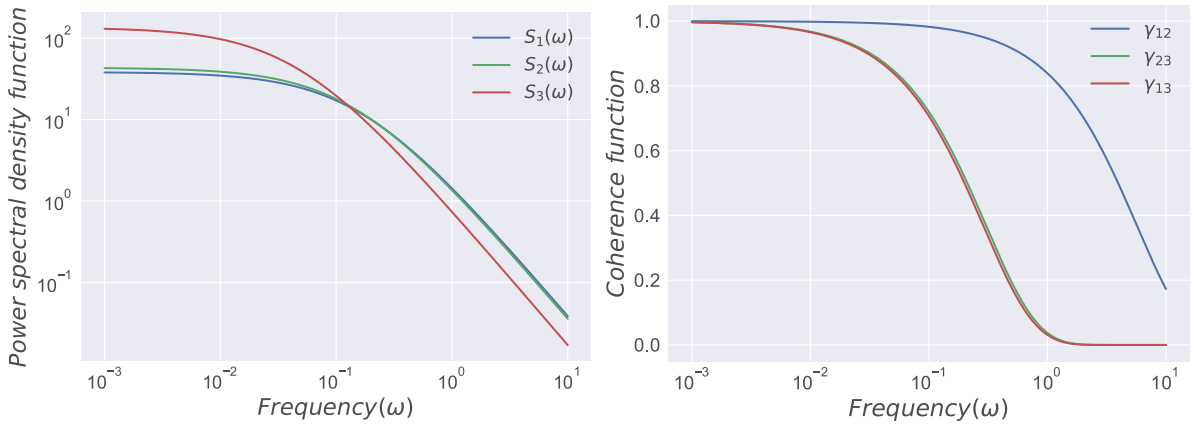

Fig. 12. Power spectra and coherence functions for a tri-variate wind velocity stochastic vector process.

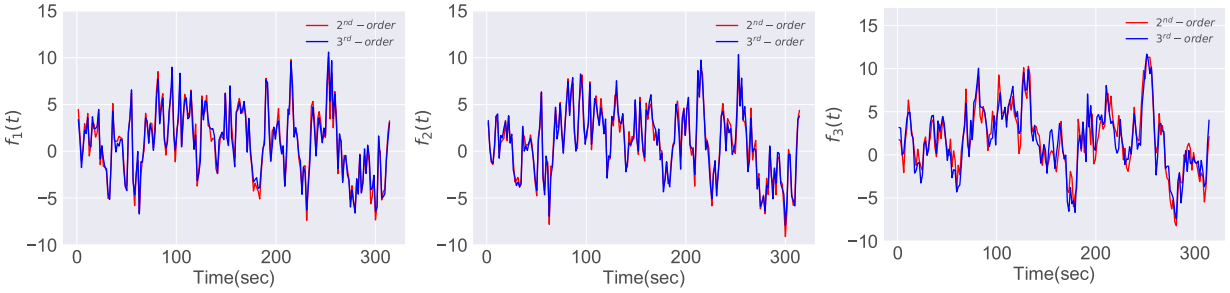

Fig. 13. Velocity histories at points 1 (left), 2 (middle) and 3 (right).

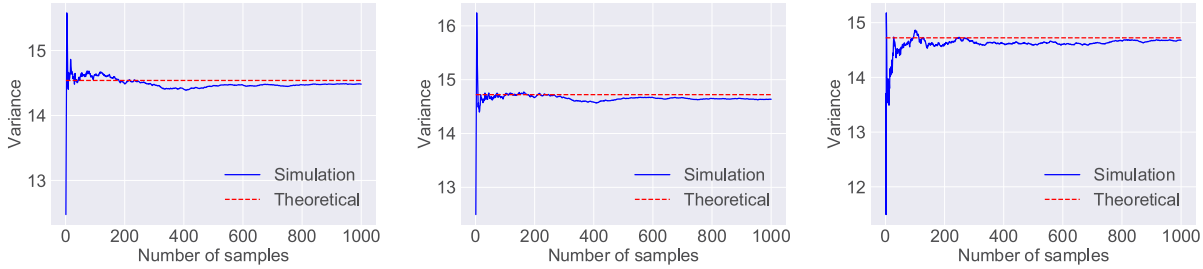

Fig. 14. Convergence of variance with increasing number of samples at points 1 (left), 2 (middle) and 3 (right).

Table 7
First order statistics of the simulated vector process.

Moments	3rd-order	2nd-order	Target
$\mathbb{E}[f_1(t)]$	−0.00143	−0.00143	0.00
$\mathbb{E}[f_2(t)]$	−0.00147	−0.00147	0.00
$\mathbb{E}[f_3(t)]$	−0.00279	−0.00279	0.00

Table 8
Second order statistics of the simulated vector process.

Moments	3rd-order	2nd-order	Target
$\mathbb{E}[f_1^2(t)]$	14.541	14.538	14.539
$\mathbb{E}[f_2^2(t)]$	14.722	14.720	14.722
$\mathbb{E}[f_3^2(t)]$	14.724	14.723	14.723
$\mathbb{E}[f_1(t)f_2(t)]$	13.698	13.697	13.698
$\mathbb{E}[f_1(t)f_3(t)]$	7.628	7.627	7.628
$\mathbb{E}[f_2(t)f_3(t)]$	8.006	8.004	8.005

target third-order moments (Table 9). The third-order simulations, on the other hand, match all moments up to third-order with high accuracy.

Table 9
Third order statistics of the simulated vector process.

Moments	3rd-order	2nd-order	Target
$\mathbb{E}[f_1^3(t)]$	4.880	0.012	4.801
$\mathbb{E}[f_2^3(t)]$	3.870	0.004	3.825
$\mathbb{E}[f_3^3(t)]$	0.337	−0.010	0.368
$\mathbb{E}[f_1(t)f_2^2(t)]$	3.938	−0.051	3.939
$\mathbb{E}[f_1(t)f_3^2(t)]$	3.218	−0.054	3.231
$\mathbb{E}[f_2(t)f_1^2(t)]$	0.931	−0.048	0.981
$\mathbb{E}[f_2(t)f_3^2(t)]$	0.297	−0.058	0.391
$\mathbb{E}[f_3(t)f_1^2(t)]$	0.435	−0.057	0.513
$\mathbb{E}[f_3(t)f_2^2(t)]$	0.140	−0.065	0.247
$\mathbb{E}[f_1(t)f_2(t)f_3(t)]$	0.355	−0.050	0.425

Finally, we present the convergence of variance and skewness with increasing number of samples and increasing number of frequency discretizations in Figs. 14–17.

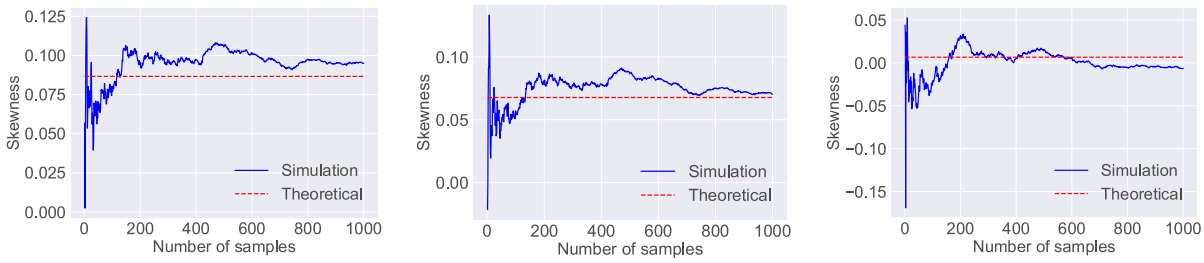

Fig. 15. Convergence of skewness with increasing number of samples at points 1 (left), 2 (middle) and 3 (right).

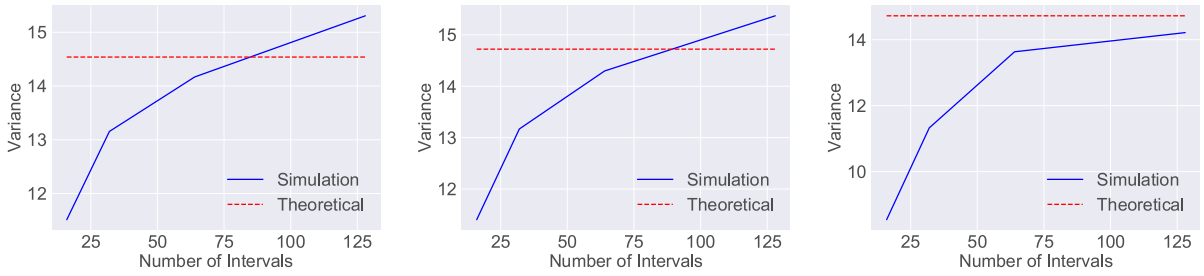

Fig. 16. Convergence of variance with increasing number of frequency discretizations at points 1 (left), 2 (middle) and 3 (right).

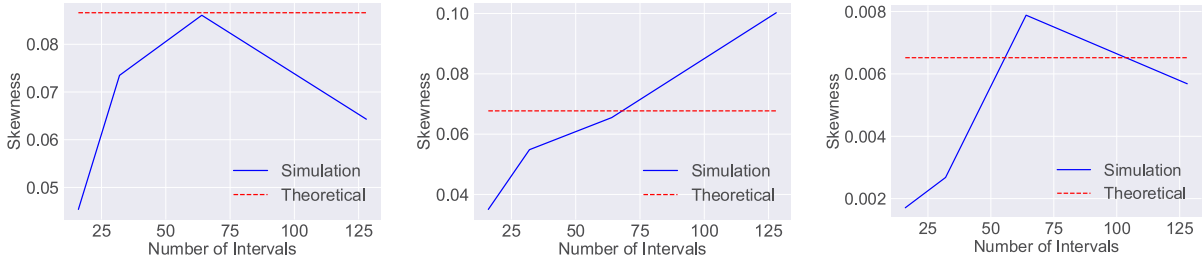

Fig. 17. Convergence of skewness with increasing number of frequency discretizations at points 1 (top), 2 (middle) and 3 (bottom).

8. Conclusions

In this paper, the 3rd-order Spectral Representation Method has been extended for the simulation of multi-dimensional random fields and ergodic, multi-variate stochastic processes. A fast Fourier transform implementation of the 3rd-order SRM has also been presented, which leads to enormous computational gains — making the generation of multi dimensional fields and multi variate processes feasible for implementation on a desktop computer. Numerical examples for the simulation of 2D and 3D random fields and the simulation of a tri-variate wind velocity stochastic process are provided, which highlight the effectiveness of the proposed methodology.

9. Software

The simulation methods discussed herein have been programmed in Python and are available in the open-source uncertainty quantification software UQpy [52].

Declaration of competing interest

The authors declare that they have no known competing financial interests or personal relationships that could have appeared to influence the work reported in this paper.

Acknowledgement

This work has been supported by the National Science Foundation under award number 1652044.

Appendix. Additional properties of random fields and random vector processes

A.1. Stationary random fields

Random fields that are invariant across the indexing variable are referred to as *stationary*. For the development of the proposed methodology we present 2 generalized notions of stationarity: strongly and weakly stationary [53].

A random field $A(x)$ is considered *strongly kth-order stationary* if the probability measure up to kth-order is invariant to a shift in index. Let $F_{A(x_1,x_2,\dots x_k)}(a_1,a_2,\dots,a_k,x_1,x_2,\dots x_k)$ denote the kth-order joint cumulative distribution function of $A(x)$ defined below as

$$F_{A(x_1,x_2,\dots x_k)}(a_1,a_2,\dots,a_k,x_1,x_2,\dots,x_k) \triangleq P[A(x_1)<a_1, A(x_2)<a_2,\dots,A(x_k)<a_k] \tag{A.1}$$

The random field is strongly kth-order stationary if

$$F_{A(x_1,x_2,\dots x_k)}(a_1,a_2,\dots,a_k,x_1,x_2,\dots,x_k) = F_{A(x_1+\xi,x_2+\xi,\dots x_k+\xi)}(a_1,a_2,\dots,a_k,x_1+\xi,x_2+\xi,\dots,x_k+\xi), \quad \forall \xi \in \mathbb{R} \tag{A.2}$$

Again, it follows that all measures of order lower than k are similarly invariant to a shift in index and that all characteristics of the kth-order joint distribution are independent of ξ. A random field is considered *strongly stationary* if Eq. (A.2) holds for all orders k.

A random field $A(x)$ is considered to be *weakly kth-order stationary* if the following conditions are met

$$\begin{aligned} &m_n^A(x_1,\dots,x_{n-1}) = m_n^A(x_1+\xi,\dots,x_{n-1}+\xi) \quad \forall n \le k \\ &\mathbb{E}[|A(x)|^n] < \infty \quad \forall n \le k \end{aligned} \tag{A.3}$$

where $m_n^A(\cdot)$ is the nth-order moment function defined in Eq. (A.5) below. For the special case of weakly 2nd-order stationary (typically referred to simply as *weakly stationary*), these conditions are:

$$\begin{aligned} &m_A(x) = m_A(x+\xi) \quad \forall \xi \in \mathbb{R} \\ &C_{A,A}(x_1,x_2) = C_{A,A}(x_1-x_2,0) \quad \forall t_1,t_2 \in \mathbb{R} \\ &\mathbb{E}[|A(x)|^2] < \infty \end{aligned} \tag{A.4}$$

where $m_A(x) = \mathbb{E}[A(x)]$ represents the mean function and $C_{A,A}(x_1,x_2) = \mathbb{E}[(A(x_1)-m_A(x_1))(A(x_2)-m_A(x_2))]$ represents the auto-covariance function. It is interesting to note that strong kth-order stationarity implies weak kth-order stationarity, whereas the converse is not necessarily true. Weakly stationary random fields are particularly important here because existing simulation methods are capable only of generating weakly 2nd-order stationary non-Gaussian random fields (Gaussian random fields are strongly stationary due to the properties of Gaussian distributions). That is, because existing expansions are derived from 2nd-order properties of the random field (i.e. power spectrum or two-point correlation), the simulated fields are, by construction, weakly stationary.

Of particular interest in this work is the notion of the weak 3rd-order stationarity, which implies that the bispectrum is invariant. As we will see, random fields generated according to the proposed method are weakly 3rd-order stationary.

A.2. Cumulants and moments of random fields

When a random field is Gaussian, the full joint probability density of the random field can be easily computed from the mean and auto-correlation function, but this is not generally true for more general cases. Nonetheless, for practical purposes, many random fields are characterized through some subset of properties of the field — typically its moments, cumulants, or spectra. These properties are briefly reviewed in the following. We note however that, given the classical moment problem, the full probability density of the random field is identifiable from the moments only when Carleman's Condition is satisfied — that is only when the infinite moment series has positive radius of convergence [54]. Consequently, moments (cumulants/spectra) provide only a limited view of the random field since we realistically cannot expect to know infinite moments, nor can we be assured that Carleman's Condition will hold.

Moments and cumulants of random variables and random vectors are not discussed here for brevity. The interested reader is referred to [14]. The nth-order moment of a stationary random field $A(x)$ is given by

$$m_n^A(\xi_1,\dots,\xi_{n-1}) = \mathbb{E}[A(x)A(x+\xi_1)\dots A(x+\xi_{n-1})]. \tag{A.5}$$

The cumulants of a stationary random field, meanwhile, can be expressed in terms of the moments by applying [55]

$$\begin{aligned} c_{k_1,k_2,\dots,k_n} &= c[X_1^{k_1},X_2^{k_2},\dots,X_n^{k_n}] \\ &= \sum(-1)^{p-1}(p-1)!E\Big[\prod_{i\in s_1}X_i\Big]E\Big[\prod_{i\in s_2}X_i\Big]\dots E\Big[\prod_{i\in s_p}X_i\Big] \end{aligned} \tag{A.6}$$

yielding the following first three cumulants:

$$\begin{aligned} &c_1^A = m_1^A \\ &c_2^A(\xi) = m_2^A(\xi) - m_1^A \\ &c_3^A(\xi_1,\xi_2) = m_3^A(\xi_1,\xi_2) - m_1^A[m_2^A(\xi_1)+m_2^A(\xi_2)+m_2^A(\xi_2-\xi_1)] + 2(m_1^A)^3 \\ &\vdots \end{aligned} \tag{A.7}$$

Notice that when $A(x)$ is a zero mean process ($m_1^A = 0$), the first three moments and cumulants are equivalent, but they differ for orders ($n \ge 4$). Non-zero higher-order cumulants indicate non-Gaussianity. In particular, odd-order cumulants give rise to asymmetric non-linearities whereas even-order cumulants give rise to symmetric non-linearities. Further details on the moment and cumulant properties of fields can be found in [14,35].

A.3. Properties of stochastic vector processes

Consider a one-dimensional, m-variate (1D-mV) 3rd-order stationary stochastic vector process $\boldsymbol{f}(t)$ with components $[f_1(t), f_2(t), \dots f_m(t)]$ having zero mean for each component, $\mathbb{E}[f_j(t)] = 0$ for $j = 1,2,\dots,m$. The second-order correlation function of this stochastic vector process is given by $R_{ij}(\tau) = \mathbb{E}[f_i(t)f_j(t+\tau)]$ for $i,j = 1,2,\dots,m$. Similarly, the third-order correlation function is given by $\mathbb{E}[f_i(t)f_j(t+\tau_1)f_k(t+\tau_2)] = R_{ijk}^{(3)}(\tau_1,\tau_2)$ for $i,j,k = 1,2,\dots,m$. Additional details regarding the shape and size of the second and third-order auto-correlation functions can be found in [49].

For real-valued, third-order stationary stochastic vector processes, the following second-order symmetry relationships hold,

$$R_{ij}(\tau) = R_{ij}(-\tau), \ i,j = 1,2,\dots,m \ ; R_{ij}(\tau) = R_{ji}(\tau), \ i,j = 1,2,\dots,m \tag{A.8}$$

and the following third-order symmetry conditions hold,

$$\begin{aligned} &R_{ijk}^{(3)}(\tau_1,\tau_2) = R_{ijk}^{(3)}(\tau_2,\tau_1), \ i,j,k = 1,2,\dots,m \\ &R_{ijk}^{(3)}(\tau_1,\tau_2) = R_{ijk}^{(3)}(-\tau_1,-\tau_2), \ i,j,k = 1,2,\dots,m \\ &R_{ijk}^{(3)}(\tau_1,\tau_2) = R_{ijk}^{(3)}(-\tau_1,-\tau_1-\tau_2), \ i,j,k = 1,2,\dots,m \\ &R_{ijk}^{(3)}(\tau_1,\tau_2) = R_{ikj}^{(3)}(\tau_1,\tau_2) = R_{jik}^{(3)}(\tau_1,\tau_2) = R_{jki}^{(3)}(\tau_1,\tau_2) \\ &= R_{kij}^{(3)}(\tau_1,\tau_2) = R_{kji}^{(3)}(\tau_1,\tau_2), \ i,j,k = 1,2,\dots,m \end{aligned} \tag{A.9}$$

The moment properties of the stochastic vector properties relate to their spectral properties through the forward and inverse Wiener-Khintchine transformations. The third-order cross spectral density can be obtained from the third-order cross auto-correlation function as follows:

$$B_{ijk}(\omega_1,\omega_2) = \frac{1}{(2\pi)^2}\int_{-\infty}^{\infty} R_{ijk}^{(3)}(\tau_1,\tau_2)e^{-\imath(\omega_1\tau_1+\omega_2\tau_2)}d\tau_1 d\tau_2 \quad \text{for } i,j,k = 1,2,\dots,m \tag{A.10}$$

where $B_{ijk}(\omega_1,\omega_2)$ is the third-order cross spectral density. Relations between other moments and spectra can be obtained similarly and can be specifically found in [49]. Additional details regarding the size and shape of the second and third order cross-spectral density can also be found in [49].

The second and third order cross spectral density functions are complex valued in general and the following symmetry conditions hold

$$\begin{aligned} &S_{jj}(\omega) = S_{jj}(-\omega),\ \ j = 1, 2, \dots m \\ &S_{ij}(\omega) = S_{ij}^{*}(-\omega),\ \ i, j = 1, 2, \dots m;\ \ i \neq j \\ &S_{ij}(\omega) = S_{ji}^{*}(\omega),\ \ i, j = 1, 2, \dots m;\ \ i \neq j \end{aligned} \tag{A.11}$$

$$B_{jjj}(\omega_1, \omega_2) = B_{jjj}(\omega_2, \omega_1); B_{jkl}(\omega_1, \omega_2) = B_{jkl}^{*}(\omega_2, \omega_1) \tag{A.12}$$

References

[1] K.R. Gurley, M.A. Tognarelli, A. Kareem, Analysis and simulation tools for wind engineering, Probab. Eng. Mech. 12 (1) (1997) 9–31.

[2] M.D. Shields, G. Deodatis, A simple and efficient methodology to approximate a general non-Gaussian stationary stochastic vector process by a translation process with applications in wind velocity simulation, Probab. Eng. Mech. 31 (2013) 19–29.

[3] S. Elgar, R. Guza, Observations of bispectra of shoaling surface gravity waves, J. Fluid Mech. 161 (1985) 425–448.

[4] K. Gurley, A. Kareem, Applications of wavelet transforms in earthquake, wind and ocean engineering, Eng. Struct. 21 (2) (1999) 149–167.

[5] G. Deodatis, Non-stationary stochastic vector processes: seismic ground motion applications, Probab. Eng. Mech. 11 (3) (1996) 149–167.

[6] J. Feng, C. Li, S. Cen, D. Owen, Statistical reconstruction of two-phase random media, Comput. Struct. 137 (2014) 78–92.

[7] M.D. Shields, P. Bocchini, G. Deodatis, Discussion of Feng et al. (2014).“Statistical reconstruction of two-phase random media”[Comput. Struct. 137 (2014) 78–92], Comput. Struct. 163 (2016) 83–85.

[8] M. Shinozuka, Monte Carlo solution of structural dynamics, Comput. Struct. 2 (5-6) (1972) 855–874.

[9] M. Shinozuka, C.M. Jan, Digital simulation of random processes and its applications, J. Sound Vib. 25 (1) (1972) 111–128.

[10] M. Shinozuka, G. Deodatis, Simulation of stochastic processes by spectral representation, Am. Soc. Mech. Eng. 44 (4) (1991).

[11] S.P. Huang, S.T. Quek, K.K. Phoon, Convergence study of the truncated Karhunen-Loeve expansion for simulation of stochastic processes, Internat. J. Numer. Methods Engrg. 52 (9) (2001) 1029–1043.

[12] R.G. Ghanem, P.D. Spanos, Stochastic Finite Elements: A Spectral Approach, Springer New York, 1991.

[13] M. Grigoriu, Probabilistic models for stochastic elliptic partial differential equations, J. Comput. Phys. 229 (22) (2010) 8406–8429.

[14] M.D. Shields, H. Kim, Simulation of higher-order stochastic processes by spectral representation, Probab. Eng. Mech. 47 (2017) 1–15.

[15] B. Puig, F. Poirion, C. Soize, Non-Gaussian simulation using Hermite polynomial expansion: convergences and algorithms, Probab. Eng. Mech. 17 (3) (2002) 253–264.

[16] Z. Liu, Z. Liu, Y. Peng, Dimension reduction of Karhunen-Loeve expansion for simulation of stochastic processes, J. Sound Vib. 408 (2017) 168–189.

[17] M. Grigoriu, Applied Non-Gaussian Processes: Examples, Theory, Simulation, Linear Random Vibration, and MATLAB Solutions, Prentice Hall, Inc, Englewood Cliffs, NJ, 1995, 1995.

[18] M. Grigoriu, Simulation of stationary non-Gaussian translation processes, J. Eng. Mech. 124 (2) (1998) 121–126.

[19] M.D. Shields, G. Deodatis, P. Bocchini, A simple and efficient methodology to approximate a general non-Gaussian stationary stochastic process by a translation process, Probab. Eng. Mech. 26 (4) (2011) 511–519.

[20] H. Kim, M.D. Shields, Modeling strongly non-Gaussian non-stationary stochastic processes using the iterative translation approximation method and Karhunen-Loève expansion, Comput. Struct. 161 (2015) 31–42.

[21] M.D. Shields, G. Deodatis, Estimation of evolutionary spectra for simulation of non-stationary and non-gaussian stochastic processes, Comput. Struct. 126 (1) (2013) 149–163.

[22] S. Sakamoto, R. Ghanem, Simulation of multi-dimensional non-gaussian non-stationary random fields, Probab. Eng. Mech. 17 (2) (2002) 167–176.

[23] B. Zeldin, P. Spanos, Random field representation and synthesis using wavelet bases, J. Appl. Mech. 63 (4) (1996) 946–952.

[24] K.K. Phoon, H.W. Huang, S.T. Quek, Comparison between Karhunen-Loeve and wavelet expansions for simulation of Gaussian processes, Comput. Struct. 82 (13–14) (2004) 985–991.

[25] M. Shinozuka, Simulation of multivariate and multidimensional random processes, J. Acoust. Soc. Am. 49 (1B) (1971) 357–368.

[26] M.P. Mignolet, P.D. Spanos, Recursive simulation of stationary multivariate random processes—Part I, J. Appl. Mech. 54 (3) (1987) 674–680.

[27] Recursive simulation of stationary multivariate random processes—Part II, J. Appl. Mech. 54 (3) (1987) 681–687.

[28] Y. Li, A. Kareem, Simulation of multivariate nonstationary random processes by FFT, J. Eng. Mech. 117 (5) (1991) 1037–1058.

[29] Y. Li, A. Kareem, Simulation of multivariate random processes: Hybrid DFT and digital filtering approach, J. Eng. Mech. 119 (5) (1993) 1078–1098.

[30] G. Deodatis, Simulation of ergodic multivariate stochastic processes, J. Eng. Mech. 122 (August) (1996) 778–787.

[31] M. Shinozuka, G. Deodatis, Simulation of multi-dimensional Gaussian stochastic fields by spectral representation, Appl. Mech. Rev. 49 (1) (1996) 29–53.

[32] R. Popescu, G. Deodatis, J.-H. Prevost, Simulation of homogeneous nonGaussian stochastic vector fields, Probab. Eng. Mech. 13 (1) (1998) 1–13.

[33] M. Shields, G. Deodatis, A simple and efficient methodology to approximate a general non-Gaussian stationary stochastic vector process by a translation process with applications in wind velocity simulation, Probab. Eng. Mech. 31 (2013) 19–29.

[34] Z. Liu, Z. Liu, Y. Peng, Simulation of multivariate stationary stochastic processes using dimension-reduction representation methods, J. Sound Vib. 418 (2018) 144–162.

[35] D.R. Brillinger, An introduction to polyspectra, Ann. Math. Stat. 36 (5) (1965) 1351–1374.

[36] C.L. Nikias, M.R. Raghuveer, Bispectrum estimation: A digital signal processing framework, Proc. IEEE 75 (7) (1987) 869–891.

[37] K. Lii, M. Rosenblatt, C. Van Atta, Bispectral measurements in turbulence, J. Fluid Mech. 77 (01) (1976) 45–62.

[38] H. Kim, Simulation of Non-Gaussian/Non-Stationary Stochastic Processes: Beyond Second-Order Orthogonality (Ph.D. thesis), Johns Hopkins Unversity, 2018.

[39] Y.C. Kim, E.J. Powers, Digital bispectral analysis and its applications to nonlinear wave interactions, IEEE Trans. Plasma Sci. 7 (2) (1979) 120–131.

[40] C. McComas, M. Briscoe, Bispectra of internal waves, J. Fluid Mech. 97 (01) (1980) 205–213.

[41] M.J. Hinich, M. Wolinsky, Normalizing bispectra, J. Statist. Plann. Inference 130 (1) (2005) 405–411.

[42] A. Hanssen, L.L. Scharf, A theory of polyspectra for nonstationary stochastic processes, IEEE Trans. Signal Process. 51 (5) (2003) 1243–1252.

[43] H. Cramér, Stationary and Related Stochastic Processes; Sample Function Properties and Their Applications, Wiley, New York, 1967.

[44] L. Vandanapu, M.D. Shields, 3rd-order spectral representation method: part i – multi-dimensional random fields with fast fourier transform implementation, 2020, arXiv:1910.06420.

[45] D. Willinger, Some history of the study of higher-order moments and spectra, in: Workshop on Higher-Order Spectral Analysis, Vol. 1, No. 2, IEEE, 1991, pp. 41–45.

[46] S.O. Rice, Mathematical analysis of random noise, Bell Syst. Tech. J. 23 (3) (1944) 282–332.

[47] R.J. Adler, Random Fields and Geometry, in: Springer Monographs in Mathematics, Springer New York, New York, NY, 2007.

[48] J.W. Cooley, J.W. Tukey, An algorithm for the machine calculation of complex Fourier series, Math. Comp. 19 (90) (1965) 297–301.

[49] L. Vandanapu, M.D. Shields, 3rd-order spectral representation method: Part II – Ergodic multi-variate random processes with fast Fourier transform, 2019, arXiv:1911.10251.

[50] J.C. Kaimal, J.C. Wyngaard, Y. Izumi, O.R. Coté, Spectral characteristics of surface-layer turbulence, Q. J. R. Meteorol. Soc. 98 (417) (1972) 563–589.

[51] A.G. Davenport, The dependence of wind load upon meteorological parameters, in: Wind Effects on Building and Structures, Univ. Toronto Press, Canada, 1967, pp. 19–82.

[52] A. Olivier, D. Giovanis, B. Aakash, M. Chauhan, L. Vandanapu, M. Shields, UQpy: A general purpose Python package and development environment for uncertainty quantification, J. Comput. Sci. 47 (2020) 101204.

[53] K.I. Park, Fundamentals of Probability and Stochastic Processes with Applications to Communications, Springer International Publishing, Cham, 2018, pp. 1–275.

[54] N.I. Akhiezer, N. Kemmer, The Classical Moment Problem: and Some Related Questions in Analysis, Vol. 5, Oliver & Boyd Edinburgh, 1965.

[55] C. Nikias, A. Petropulu, Higher-order Spectra Analysis: A Nonlinear Signal Processing Framework, in: Prentice Hall Signal Processing Series, PTR Prentice Hall, 1993.